Research and Development on Critical (Sonic) Flow of Multiphase Fluids through Wellbores in Support of Worst-Case-Discharge Analysis for Offshore Wells

**Mewbourne School of Petroleum and
Geological Engineering
The University of Oklahoma, Norman
100 E Boyd St. Norman, OK-73019**

The UNIVERSITY *of* OKLAHOMA

March 24, 2018

This page intentionally left blank.

Research and Development on Critical (Sonic) Flow of Multiphase Fluids through Wellbores in Support of Worst-Case-Discharge Analysis for Offshore Wells

Authors:

Saeed Salehi, Principal Investigator
Ramadan Ahmed, Co- Principal Investigator
Rida Elgaddafi, Postdoctoral Associate
Raj Kiran, Research Assistant

The UNIVERSITY *of* OKLAHOMA

For: The US Department of the Interior
Bureau of Ocean Energy Management Gulf of Mexico OCS Region

BOEM
BUREAU OF OCEAN ENERGY MANAGEMENT

This page intentionally left blank.

DISCLAIMER

Table of Contents

List of Figures

List of Tables

Nomenclature

Abbreviations and Acronyms

A_g	Gas inlet area
A_{total}	Total area of the inlet cross-section
AN	Annular flow
BB	Bubble flow
CFD	Computational fluid dynamics
CH	Churn flow
DB	Dispersed bubble flow
E	Specific energy
$\vec{F}$	External body forces
$\vec{F}_i$	External force
$\vec{F}_{lift,i}$	Lift force
$\vec{F}_{vm,i}$	Virtual mass force
$\vec{g}$	Acceleration due to gravity
I	Unit tensor
INT	Intermittent
k_{eff}	Effective thermal conductivity
k_t	Turbulent thermal conductivity
Ma	Mach number
$\dot{m}_{ij}$	Mass transfer from phase i to j
$\dot{m}_{ji}$	Mass transfer from phase j to i
MUSCL	Monotone Upstream-Centered Schemes for Conservation Laws
p	Static pressure
PISO	Pressure-Implicit with Splitting of Operators
PRESTO	PREssure STaggerring Option
QUICK	Quadratic Upstream Interpolation for Convective Kinematics
Rij	Interaction force between phases
RSM	Reynold Stress Model
RNG	Re-Normalization Group
SL	Slug
S_E	Volumetric heat resources
S_{α_i}	Source term
S_h	Source term for heat transfer in the energy equation
S_m	Source term for mass added to the continuous phase from the dispersed phase
SST	Shear Stress Transport
T	Temperature
$\vec{v}$	Velocity vector

V_i	Total volume of ith phase
V_l	Superficial liquid velocity
V_{SL}	Superficial liquid velocity
V_g	Assigned inlet gas velocity for the model
V_{SG}	Superficial gas velocity
V_{g_given}	Specified superficial gas velocity
WCD	Worst case discharge

Greek Symbols

ρ	Density (kg/m^3)
σ	Surface tension
$\bar{\bar{\tau}}$	Stress tensor
μ	Molecular viscosity
ρ_i	Density of ith phase
α_i	Volume fraction of ith phase
ρ_m	Density of the mixture (kg/m^3)

Executive Summary

This report presents results of a Computational Fluid Dynamics (CFD) study and a review of two-phase fluid flow modeling in pipe and annulus. This work is performed under BSEE/BOEM-contract No. M16PS00059. The study focuses on: i) theory of CFD modeling; ii) review of CFD modeling in pipe and annulus; iii) CFD model development and validation; and iv) CFD simulation for low and high Mach number two-phase flows. In the first section of this report, a brief outline of different modeling techniques implemented in ANSYS Fluent is illustrated. The second part highlights the past modeling work performed by researchers for fluid flow in pipe and annulus. With this background, the results and discussion of the current simulation work are presented, and interpretations are made.

The modeling work section establishes the understanding of the fluid flow phenomenon in annulus and pipe where a different set of methods can be implemented. In pursuit of development of theoretical knowledge of CFD modeling in ANSYS Fluent, a thorough review of ANSYS models was conducted. The study suggests that, out of three multiphase models, Volume of Fluid (VOF) and Eulerian models are the best suited for current research. VOF model is computationally less expensive and can provide reasonable results for lower velocities while the Eulerian model is best suited for annular flow regime and can capture the flow effects in the flow system more efficiently. The k-ε turbulent model is best suited for incompressible flow while the k-ω models are generally used in the case of compressible flow.

With this understanding, the CFD modeling was conducted for a broad range of past experimental data. Two types of geometries were considered: (a) flow in the pipe; and (b) flow in the annulus. Mostly VOF model was used for incompressible pipe and annular flows. In some cases, the Eulerian model was used for the annulus. Finally, the current high-velocity experimental set-up available at the University of Oklahoma was simulated using Eulerian model. Since the experiments will be carried out at high velocity, the role of compressibility cannot be neglected. Therefore, a set of cases were simulated using high inlet pressure to obtain high velocity in the test section. Simulation results show that high-Mach number can be achieved at the exit. Besides this, pressure sharply decreased close to the exit indicating the presence of considerable gas expansion.

1. Introduction

1.1 Background

CFD modeling is a robust method to address the problems of multiphase fluid flow characterization; however, the mathematical treatment of every flow system is different from each other. Each problem exhibits unique characteristics, and there is a lack of a generalized model for multiphase flow. Hence, it becomes critical to apply and develop the technical understanding to resolve a particular multiphase flow problem. This technical understanding is based on quantifying the physics of the flow, setting up appropriate geometry and boundary conditions, and capturing the results appropriately. The physics of the flow refers to the required models such as for interphase momentum transfer whether the drag force will induce considerable error in the solution or not. Likewise, geometry has a significant impact on the models. An appropriate boundary condition is required to resolve the flow characteristics corresponding to the problem. Otherwise, the results do not describe the flow adequately. Hence, it becomes crucial to understand the parameters that can be obtained while solving the problems. Accuracy comes with the cost, and CFD modeling is computationally intensive approach, so it is of paramount importance that correct approach should be adopted to address a particular problem. In case of worst case discharge (WCD) calculation, pressure variation with depth is the most critical aspect to be looked into using CFD models.

The current study is focused on multiphase flow in pipes and annuli. The flow characteristics are different in both geometries. The presence of two boundaries exacerbates the problem of flow in the annulus with respect to turbulence in the system. In addition, high velocity leads to dominant compressibility effect of gas, resulting in a change in discharge properties of the fluid at the exit. Hence, the isothermal flow assumption may not be valid. The CFD modeling can be used in verification of the upscaling of the experimental results to field conditions.

1.2 Problem Statement

There have been several limitations of existing CFD modeling to characterize multiphase flows in wellbore conditions. The most prominent one is the unavailability of high-velocity simulation. In addition, the effect of geometry is not yet thoroughly studied. The effect of compressibility is not included in the past CFD studies of oil and gas industry (Parsi et al., 2015 and Zabaras et al., 2013). Most of the studies considered a constant pressure gradient for particular flow pattern, which may not be the case with the high-velocity flows (Hasan and Kabir, 1990 and Caetano et al., 1992). It has also been observed in the past that modeling work is based on isothermal condition, which is not suitable for worst case discharge scenario (Parsi et al., 2015). Overall, the WCD model needs to account for these underlying limitations of the current models.

2. Theory of CFD Modeling

2.1. Multiphase Flow

The petroleum industry deals with several types of fluids including oil, gas, and drilling and fracturing fluids (Barati and Liang, 2014; Torsvik et al., 2017 and Hulsurkar et al., 2018). These fluids have different properties, and consequently, they have different flow characteristics. Furthermore, the traveling of two distinct phases together complicates the flow characteristics (Shirdel and Sepehrnoori, 2017). For example, oil and gas traveling through production systems often exhibit complex multiphase flow characteristics. Different modeling approaches (empirical, analytical, mechanistic, and numerical methods) have been developed for modeling multiphase flows (Ibarra et al., 2017; Caetano et al., 1992 and Mukherjee and Brill, 1985). The empirical models are based on experimental observations and correlations derived from measurements (Duns and Ros, 1963; Orkiszewski, 1967 and Mukherjee and Brill, 1985). The analytical models are based on the physics of the flow phenomenon. However, several aspects of the fluid flow are simplified to obtain a closed form solution to the problem (Zuber and Findlay, 1965). The mechanistic models are a combination of empirical analysis and analytical treatment of the models (Hasan and Kabir, 1990 and Caetano et al., 1992). The most advanced form of the theoretical model for the flow characterization is the numerical approach (Parsi et al., 2015). Though the numerical method is computationally intensive, it gives a better characterization of the flow. In the numerical techniques, there are several approaches which have been accounted in the past research.

With respect to our current study, the CFD study includes modeling effort using ANSYS Fluent. Hence, in this section, different mathematical models used in ANSYS Fluent for flow characterization has been discussed (Fluent, 2016a).

2.2. CFD Models

CFD uses different approaches for fluid flow characterization. ANSYS Fluent uses various methods to obtain numerical solutions to the fundamental conservation equations of mass, momentum, and energy. The basic equation for mass is given by:

$$\frac{\partial \rho}{\partial t} + \nabla.(\rho \vec{v}) = S_m \tag{2.1}$$

where, ρ is the density, $\vec{v}$ is the velocity vector, and S_m is the source term for mass transferred to the continuous phase from the dispersed phase. The conservation of momentum equation is expressed as:

$$\frac{\partial (\rho \vec{v})}{\partial t} + \nabla.(\rho \vec{v} \vec{v}) = -\nabla p + \nabla.(\bar{\bar{\tau}}) + \rho \vec{g} + \vec{F} \tag{2.2}$$

where p is static pressure, $\vec{g}$ is the acceleration due to gravity, $\vec{F}$ is external body forces, $\bar{\bar{\tau}}$ is stress tensor which is given by Eqn. (2.3).

$$\bar{\bar{\tau}} = \mu \left[(\nabla \vec{v} + \nabla \vec{v}^T) - \frac{2}{3} \nabla . \vec{v} I \right] \tag{2.3}$$

where μ is the molecular viscosity and I is unit tensor.

With the knowledge of these two essential equations, we need to understand the numerical methods of ANSYS Fluent. It uses two types of models for multiphase flow analysis: Eulerian-Lagrangian and Eulerian-Eulerian. The Eulerian-Lagrangian models are applied for discrete phase modeling in which continuous phase treated as a continuum, and dispersed phase flow is solved by tracking a large number of bubbles or droplets. The dispersed phase can exchange momentum, mass, and energy with the continuous phase. This method is not suited for flows in which the volume fraction of the second phase is considerable. However, it is well suited for problems like spray dryer and fuel combustion. In this study, since both phases (liquid and gas) have equal importance, hence such modeling strategy cannot be applied.

On the other hand, Eulerian-Eulerian approach treats different phases as interpenetrating continua using the concept of phasic volume fraction. The idea of phasic volume fraction relies on the premise that the volume fractions are a continuous function in the spatial and temporal domain and the total sum of the volume fraction of all phases are unity. Conservation principles are applied for each phase and equations are closed by empirical correlations or use of the kinetic theory. The Eulerian-Eulerian approach has three modeling formulations: mixture model, volume of fluid (VOF) model, and Eulerian Model. The mixture model considers the phases as interpenetrating continua and uses momentum equation for the mixture as a whole and recommends relative velocity of dispersed phase. The VOF model is a surface tracking technique implemented for immiscible fluids in which the fluid interface is studied. Single momentum equation is used, and the volume fraction of each phase in each cell is tracked. For bubble flow with dispersed phase volume exceeding 10%, mixture or Eulerian model is preferred. Slug flow can be simulated using VOF model. In case of widely distributed dispersed phase flow, the mixture model is suitable. For a flow with dispersed phase concentrated in a specific zone, the Eulerian model is chosen. Eulerian model is ideal in the case of known interphase drag laws; however, when the interphase drag is unknown, the mixture model should be preferred. Eulerian model is computationally intensive than other models. For accuracy, Eulerian is suitable while for computational stability the mixture model is favored.

2.2.1. Mixture Model

Mixture models are based on the analysis of multiphase fluid considering the whole fluid as single phase using the concept of slip velocities (relative velocities). Accordingly, the phases are assumed to move at the same velocity, and the model becomes a homogenous multiphase model. The governing equations consist of continuity, momentum, energy equations for the mixture, volume fraction for the secondary phase and algebraic expressions for relative velocities. The model is used in different ways to model multiphase flows (Hohne and Lucas, 2011, Li et al., 2008).

Governing equations

The Continuity equation for mixture model is given as:

$$\frac{\partial}{\partial t}(\rho_m) + \nabla \cdot (\rho_m \overrightarrow{v_m}) = 0 \tag{2.4}$$

where v_m is the mixture velocity or mass average velocity, ρ_m is the density of the mixture. Mass average velocity is calculated using following equation:

$$\overrightarrow{v_m} = \frac{\sum_{k=1}^{n} \alpha_k \rho_k \overrightarrow{v_k}}{\rho_m} = \frac{\alpha_g \rho_g \overrightarrow{v_g} + \alpha_l \rho_l \overrightarrow{v_l}}{\alpha_g \rho_g + \alpha_l \rho_l} \tag{2.5}$$

Mixture density is given by:

$$\rho_m = \sum_{k=1}^{n} \alpha_k \rho_k \tag{2.6}$$

where α is volume fraction, ρ is density. Subscript k represents different phases of the mixture, g refers to gas and l refers to the liquid phase. Momentum equation can be written as:

$$\frac{\partial}{\partial t}(\rho_m \overrightarrow{v_m}) + \nabla \cdot (\rho_m \overrightarrow{v_m} \overrightarrow{v_m}) = -\nabla P + \nabla \cdot \left[\mu_m \left(\nabla \overrightarrow{v_m} + \nabla \overrightarrow{v_m}^T \right) \right] + \rho_m \vec{g} + \nabla \cdot \{ (\alpha_g \mu_g +$$
$$\alpha_l \mu_l) \overrightarrow{v_{dr}} \overrightarrow{v_{dr}} \} \tag{2.7}$$

where the viscosity of the mixture (μ_m) is calculated by the following equation:

$$\mu_m = \alpha_g \mu_m + \alpha_l \mu_l \tag{2.8}$$

Drift velocity ($\overrightarrow{v_{dr}}$) takes the following form in mixture model:

$$\overrightarrow{v_{dr}} = \overrightarrow{v_k} - \overrightarrow{v_m} \tag{2.9}$$

where $\overrightarrow{v_k}$ is the velocity of one phase. The energy equation for mixture model is represented by following equation:

$$\frac{\partial}{\partial t} \sum_{k=1}^{n} (\alpha_k \rho_k E_k) + \nabla \cdot \sum_{k=1}^{n} (\alpha_k \overrightarrow{v_m} (\rho_k E_k + p)) = \nabla \cdot [k_{eff} \nabla T] + S_E \tag{2.10}$$

where k_{eff} is the effective conductivity, k_t is turbulent thermal conductivity, S_E is volumetric heat resources.

2.2.2. Volume of Fluid (VOF) Model

In VOF model, two or more phases can be handled. The equations of motion are solved applying the boundary conditions, and the volume fraction of each phase is tracked. It can be applied for the steady or transient tracking of any gas-liquid interface, and for the motion of large bubbles in the liquid. The governing equations used in this model are continuity and momentum equations. The continuity equation for the secondary phase is solved to characterize the development of an interface with space and time. For the ith phase, the continuity equation can be written as follows:

$$\frac{1}{\rho_i} \left[\frac{\partial}{\partial t}(\alpha_i \rho_i) + \nabla \cdot (\alpha_i \rho_i \overrightarrow{v_i}) = S_{\alpha_i} + \sum_{i=1}^{n} (\dot{m}_{ij} - \dot{m}_{ji}) \right] \tag{2.11}$$

where ρ_i is the density of ith phase, α_i is the volume fraction of ith phase, $\dot{m}_{ij}$ refers to mass transfer from phase i to j and $\dot{m}_{ji}$ refers to mass transfer from phase j to i, S_{α_i} is the source term. Once the volume fraction for the secondary phase is obtained, the volume fraction of primary phase is determined by using the constraint, which suggests that the sum of the volume fraction of each phase is unity. The material properties are calculated using mixture rule which can be represented by the following equation:

$$\rho = \Sigma \alpha_i \rho_i \tag{2.12}$$

The VOF model considers the general momentum equation for a solution which is depicted in Eqn. (2.2). The momentum equation is solved for shared velocity among phases which makes the model vulnerable to substantial velocity differences between the phases. Likewise, the momentum and energy equations are also shared between the phases which leads to similar problem of inaccuracy when the difference between the temperatures of the phases are substantial. The energy equation for VOF model can be represented as follows:

$$\frac{\partial}{\partial t}(\rho E) + \nabla \cdot \left(\vec{v}(\rho E + p) \right) = \nabla \cdot \left(k_{eff} \nabla T \right) + S_h \tag{2.13}$$

where E is the specific energy, T is the temperature, k_{eff} is the effective thermal conductivity, S_h is the source term.

2.2.3. Eulerian Models

Eulerian model is the most advanced model in CFD, which can model several secondary phases but can be limited by memory size of the computational facility and convergence behavior the governing equations. The Eulerian treatment of each phase is based on two considerations. All phases share single pressure, and momentum and continuity equations are solved for each phase. The numerical model considers the concept of phasic volume fractions and conservation equations are satisfied for each phase individually. The solution of these equations involves instantaneous mass balance for each phase. The volume of ith phase is given by the following equation:

$$V_i = \int \alpha_i dV \tag{2.14}$$

where α_i refers to the volume fraction of ith phase. V_i is the total volume of ith phase. In addition, it is assumed that the sum of volume fraction for each phase will be unity. The basic conservation equations include mass, momentum, and energy. The conservation of mass for ith phase yields

$$\frac{1}{\rho_i} \left[\frac{\partial}{\partial t}(\alpha_i \rho_i) + \nabla \cdot (\alpha_i \rho_i \vec{v_i}) = S_{\alpha_i} + \Sigma_{i=1}^n (\dot{m}_{ij} - \dot{m}_{ji}) \right] \tag{2.15}$$

Similarly, the momentum balance equation is

$$\frac{\partial(\alpha_i \rho_i \vec{v}_i)}{\partial t} + \nabla \cdot (\alpha_i \rho_i \vec{v}_i \vec{v}_i) = -\alpha_i \nabla p + \nabla \cdot (\bar{\bar{\tau}}) + \alpha_i \rho_i \vec{g} + \Sigma_{i=1}^n (R_{ij} + \dot{m}_{ij} \vec{v}_{ij} - \dot{m}_{ji} \vec{v}_{ji}) + (\vec{F}_i + \vec{F}_{lift,i} + \vec{F}_{vm,i}) \tag{2.16}$$

where Rij is interaction force between phases, $\vec{F}_i$ is the external force, $\vec{F}_{lift,i}$ is the lift force, $\vec{F}_{vm,i}$ is the virtual mass force. The interphase velocity is based on the velocity of transferred phase. The conservation of energy equation is given by:

$$\frac{\partial(\alpha_i \rho_i h_i)}{\partial t} + \nabla.(\alpha_i \rho_i \vec{u}_i h_i) = \alpha_i \frac{\partial p_i}{\partial t} + \bar{\bar{\tau}}.\nabla \vec{u}_i - \nabla.\vec{q}_i + S_i + \sum_{i=1}^{n}(Q_{ij} + \dot{m}_{ij} h_{ij} - \dot{m}_{ji} h_{ji}) \quad (2.17)$$

2.2.4. Turbulent Models

The multiphase flow problem becomes complex due to the presence of turbulence in the system. There are several options provided in ANSYS Fluent to address this aspect of multiphase flow. One of the widely used turbulent models for air-water flow is the k−ε model. In the k−ε model, k and ε refer to the turbulent kinetic energy and dissipation rate, respectively. The model contains two transport equations and has three types of formulations: standard, RNG, and realizable. The three formulations have similar forms in terms of transport equations; however, they differ from each other in terms of calculation methodology for turbulent viscosity, Prandtl numbers, and evolution terms in dissipation rate equation. The standard k- ε model calculates the turbulent viscosity by using the values obtained for k and ε from transport equations. The model uses widely accepted constants which are derived based on extensive turbulent flow experiments to characterize shear flows and turbulence. The RNG model is a variation of the standard model, which has significant improvement in ε equations. This reflects in its effectiveness for modeling highly strained flows and useful in prediction of swirling motion and low Reynold number flows. Another turbulent model for k- ε model is realizable, which has improved performance for certain kind of flows such as complex shear flow, boundary layer separation.

Another type of turbulent model is k-ω, which is useful for simulating flow separation and flows involving heat transfer. The model has similar kinetic energy equation while ε is replaced with the equation of ω. Three formulations are developed for this type of turbulent model: (a) standard, (b) shear stress transport model (SST), and (c) Reynold stress model (RSM). The SST model has two hybrid equations developed by combining the k-ε and k-ω models. k-ω models are sensitive to boundary wall. It has been reported that the SST k-ω model is useful for simulating compressible flow while the performance of k-ε realizable is better for incompressible multiphase flow. Rui and Xing (2011) used k- ω turbulent model to simulate the supersonic cross-flow with evaporating water droplets. The SST k- ω model can describe high turbulence levels with strong acceleration; and hence, it is well-suited for high-velocity flow (Menter, 1994).

2.2.5. Comparative Analysis of Models

The review of the theoretical background of ANSYS Fluent suggests that the VOF model can be used to replicate the fluid characteristics in low-velocity conditions while the Eulerian model is preferred for high-velocity flow. In addition, the k-ε model can be used with VOF and Eulerian both for characterization of turbulence in the system. However, the k-ω model is most suited to incorporate compressibility effect in the Eulerian model. The energy equation is not required for the low-velocity condition, but at high velocity, the impacts of temperature and gas expansion

cannot be neglected. Hence, the energy equation is necessary for high Mach number fluid flow simulations.

When the flow reaches high Mach number (Ma > 0.3), Reynolds number usually becomes very high and viscous regions becomes very thin. Consequently, the fluid flow behaves as non-viscous in most part of the flow domain. This effect causes numerical instability in the model calculation. The problem is generally addressed by tuning the under-relaxation factor (Versteeg and Malalasekera, 2007). In our study, we have modified the under-relaxation factor to manage the divergence issues, and it is presented in Section 4.3. Apart from that, another critical problem is the description of gas behavior. At high pressure, the ideal gas equation may not be valid. In ANSYS Fluent, the gas behavior can be incorporated using the real equations of state. The most widely accepted equation of state, Peng-Robinson equation is used in our study. Also, the viscosity of gas cannot be assumed to be constant in the case of high-velocity. The Sutherland's viscosity equation is applied to specify the viscosity of gas in the compressible flow domain. Sutherland's viscosity law considers the kinetic theory of ideal gases and an idealized intermolecular force potential and defines the relation between dynamic viscosity and absolute temperature (Hossain et al., 2013).

3. Literature Survey

CFD is a commonly applied method for understanding the motion of fluids. Due to its flexibility and efficiency in reducing the effective design cost and its capability in simulating two-phase flow, CFD is widely employed in various industrial applications. In the area of processing industries, CFD techniques are extensively applied to study the design of different equipment and assess their performance under various conditions. For instance, the CFD applications in chemical processing industries including drying, combustion, separation, heat exchange, mass transfer, reaction, mixing, multiphase systems and material processing. Currently, commercial CFD software (ANSYS CFX, and ANSYS Fluent CFD) are generally used in several industries as well as academic institutes to have a better understanding of the flow behavior including supersonic and hypersonic flow of gases, in particular, those experiments associated with high-cost expenses (Hoque and Kalita, 2014). ANSYS CFX is a sub-module of ANSYS workbench that can deal with wide-range of fluid flow problems. It has several physical models complemented with extensive capabilities for automation and customization. Another module of ANSYS is Fluent that can address more complex fluid flow problems and have a broader list of sub-models which can cater with different properties of flow characteristics such as turbulence, heat transfer, chemical kinetics, and properties of fluids. It has been extensively used in wide range of industrial problems such as supersonic flow conditions in aviation, combustion in furnaces, and nuclear system. Therefore, CFD is considered as an alternative tool to study complex phenomena where performing experimental work might not be possible due to the limitation of equipment or technique.

In the early 1970s, most of the numerical algorithms were developed as an alternative tool for the execution of the physical experiments. Afterward, advanced techniques have been added and more comprehensive models have been developed to improve the capability of CFD codes and packages to accurately simulate the complex fluid flow problems (Hernandez-Perez, 2008). The use of commercial CFD software has been accepted by the majority of researchers around the world. CFD software can model flows in complex geometry in which complete details of flow characteristics are needed. In addition, the fluid flow associated with other phenomena, such as chemical reactions, turbulence, multiphase, and heat transfer can be simulated by the commercial CFD packages currently offered in the open market.

There are different types of turbulent and multiphase flow models that are available in the literature. The multiphase flow analysis techniques are generally classified into two main solution methodologies: i) Eulerian-Lagrangian (E-L) approach and ii) Eulerian-Eulerian (E-E) methods. In the Euler-Lagrange approach, the continuous phase is considered as a continuum and the Navier-Stokes equations are applied, whereas the solution for the dispersed phase is obtained by tracking a large number of bubbles or droplets through the calculated flow field. The dispersed phase exchanges momentum, mass, and energy with the continuous phase.

One interesting feature of Euler-Lagrange model is that its ability to capture the dispersed fluid dynamics accurately. However, the computational cost of this approach increases proportionally with the increase in the number of dispersed bubbles and droplets. Consequently, the application of this approach to simulate two-phase flow is limited to flows with low dispersed phase fractions (less than 10%) (Ben Mahmud, 2012). More details of the Euler-Lagrange approach is provided in ANSYS guide.

Since the Eulerian-Eulerian approach is adopted in this project for simulating two-phase flow characteristics in vertical pipe and annulus, details of this approach are discussed in this report. In the Eulerian-Eulerian method, different phases are mathematically modeled as interpenetrating continua in which the space of computational domain can't be occupied by more than one phase. Accordingly, the concept of phasic volume fraction is utilized. Conservation equations are formulated for each phase in order to build a set of equations. The solutions of these equations are obtained by incorporating empirical correlations. In ANSYS Fluent, the Eulerian-Eulerian multiphase model consists of three different sub-models which are defined as: i) Volume of Fluid (VOF) model; ii) mixture model; and iii) Eulerian model. The applicability of each model is governed by the complexity of the simulated phenomena.

VOF model is defined as interface tracking tool that captures the interface between two phases. The model is formulated to simulate two or more immiscible fluids in which the description of the interface between the two phases is necessary. In the model, the test fluids are described by the same single set of momentum equations and volume fraction of each phase in the computational cell is tracked throughout the domain. The model is considered as the best alternative for simulating stratified flow, free-surface flows, and steady and transient tracking of any gas-liquid interface (ANSYS Fluent 12.0 guide). A number of studies have used VOF model for simulating various flow patterns of gas-liquid flows including bubble, churn and slug flows.

The second type of Eulerian-Eulerian multiphase model is known as the mixture model. It is considered as one of the simplified multiphase flow modeling approaches, which can be applied to simulate two phases having the same or different velocities; however, it assumes local equilibrium condition within small spatial length scales. The model treats both phases (continuous and dispersed) as a single phase. Unlike other multiphase flow approaches, none of the interphase forces such as the hydrodynamic drag and lift, and virtual mass forces are considered in the mixture model. In addition, the conservation equations such as continuity, momentum, and energy equation are solved for the mixture phase. The volume fraction equation is solved for the secondary phase. The model framework is based on the assumption that all phases share the same domain and the phases may blend as they travel all the way through the flow geometry. In order to efficiently simulate the coupling among the phases, it is essential to specify interphase forces such as drag, lift, and virtual mass. Comparing with VOF and Eulerian-Lagrangian approaches, the Eulerian-Eulerian model is considered as the best option for modeling flow systems, which contain high volume fractions of the dispersed phase. However,

in describing the complex phenomena occurring at the particle-level, Eulerian-Eulerian method is less accurate than the Eulerian-Lagrangian method.

Considering various multiphase flow models offered in ANSYS software package, the volume of fluid (VOF) model is regarded as the most broadly used model. The superior performance of VOF model is due to its gas-liquid interface tracking proficiencies. In addition, sharp interfaces between two phases (gas-liquid or solid-liquid) can be determined by using these techniques. Hence, it has been widely employed to predict the flow patterns (fluid flow behavior) and also to obtain a quantitative comparison. However, Parsi et al. (2015) stated that the use of VOF approach is limited to small diameter pipes and lower superficial velocities. Furthermore, the formulation of VOF approach doesn't account for the slippage velocity between the two phases due to shared momentum concept. A detailed literature survey regarding applying different CFD models to simulate the upward two-phase flow into vertical pipe and annulus is discussed in the following section.

3.1. CFD Modeling of Flow in Pipe

For large diameter pipes (greater than 6 in), numerous CFD models (Zabaras et al., 2013; Waltrich et al., 2015; Chen, 2004; Sanati, 2015) were developed to predict two-phase flow characteristics including flow pattern, pressure loss, volumetric liquid holdup, and void fraction using multiphase flow approaches. Due to the wide use of bubble column reactors in industrial applications, Chen (2004) numerically modeled flow in bubble column reactors. Two different multiphase models (Eulerian and Algebraic Slip Mixture Model) were applied to carry out the simulation. Details of the two models including a set of conservation equations are presented in the original reference. In the Eulerian-Eulerian approach, the turbulent behavior of the liquid phase is modeled via a set of modified k-ε equations with additional terms that account for interphase turbulent momentum transfer. Correlations developed from the theory of the dispersion of discrete particles in homogeneous turbulence were used to describe turbulence in dispersed bubbly flows. In the Algebraic Slip Mixture Model, the turbulent k-ε model is applied to the mixture phase. The CFD model explicitly accounted for bubble breakup and coalescence with the implementation of Bubble Population Balance Equation (BPBE). For superficial gas velocity of 0.1 m/s (0.328 ft/s), a 15 % discrepancy in void fraction was observed between CFD prediction and experimental data.

Zabaras et al. (2013) experimentally investigated vertical two-phase flow (air-water) in large diameter pipe that has 11-inch inner diameter and 40-ft length. During the experiment, four distinct flow patterns were detected, including bubble, churn, churn-semi-annular, and semi-annular flow. To demonstrate the capability of CFD in capturing the dynamics of gas-liquid flows in large diameter pipes, a CFD model was built using ANSYS fluent to reproduce their experimental data. Two different multiphase models (transient VOF and Eulerian-Eulerian models) were used in the study. Their CFD simulation was validated in two steps: i) against the Taylor bubble where the velocity prediction of the single bubble was compared with existing experiment and correlations available in the literature, and ii) against their flow loop

measurement and OLGA simulator predictions. The accuracy of the model was found satisfactory.

Recently, Waltrich et al. (2015) experimentally investigated two-phase flow characteristics (flow patterns, pressure loss, and liquid holdup) in large diameter pipes. Concurrently, they developed CFD model to reproduce their experimental measurements. Additionally, the model predictions were validated with a number of existing experimental measurements (Asheim, 1986; Ali, 2009; and Zabaras et al., 2013) to assess the accuracy of VOF model. In the study, the pipe sizes employed in the simulations were ranged from 1 to 12.2 in and the flows of different test fluids (air-water; gas-oil and nitrogen-naphtha) were simulated. The simulation conditions were varied from standard atmospheric pressure to high-pressure and temperature. The comparative study was limited to the pressure drop data, and no liquid holdup comparison was reported. Three multiphase flow models available in ANSYS package (VOF; Eulerian combined with multi-fluid VOF (Hybrid) and mixture models) were used in the study. VOF model showed an acceptable accuracy with a maximum discrepancy of ± 20% when its predictions were compared with lab and field measurements (Waltrich et al., 2015; Asheim, 1986). The possible explanation for the discrepancies of model predictions from experimental data is that VOF model does not account for high-slip ratio due to its momentum equation sharing concept. On the other hand, the authors used the hybrid model to simulate pressure drop data at high slip ratios measured by Zabaras et al. (2013). A reasonable agreement was observed between simulation predictions and experimental data in which the discrepancy ranges from 2 to 50% corresponding to slip ratio ranging from 20 – 309. For assessment purpose, Waltrich et al. (2015) reported that hybrid model exhibited a high accuracy of pressure drop prediction compared to VOF model. However, it requires more input from the users, and it is less stable than VOF. The results showed that the mixture approach is less accurate than VOF and hybrid models in most of the simulated cases of large diameter pipes.

Sanati (2015) simulated air-water flows in the vertical pipe using K-ε turbulent model. The mixture approach was used to predict pressure gradient across the simulated test section. Model predictions were compared with experimental data (Ohnuki and Akimoto 2000). The simulated test section consisted of 8 in (0.2 m) inner diameter and total vertical length of 39 ft (12.3 m). The simulation was conducted considering a wide range of superficial gas velocity (0.03 – 4.7 m/s) and superficial liquid velocity (0.18 – 1.06 m/s). A number of empirical correlations (Duns and Ros, 1963; Orkiszewski, 1967; Hasan and Kabir, 1988 and 1990; Mukherjee and Brill, 1985) developed to predict flow pattern were incorporated in the model. Comparison of simulation results and measurements showed discrepancy ranging from 4 to 61%. Underestimation of pressure drop obtained from mixture approach has been found consistent with previous findings of Waltrich et al. (2015).

Yancheshme et al. (2016) developed CFD simulation to investigate the churn flow regime in a bubble column reactor consisted of 19-in (0.49 m) diameter and 11 ft (3.6 m) long section. Air and water were used as the dispersed and continuous phases, respectively. The superficial gas

velocity of 0.14 m/s (459 ft/s) was used. The Eulerian-Eulerian framework was applied to simulate the flow. All the simulations were performed using transient solver with the aid of ANSYS Fluent 14.5. The simulation results are validated with experimental measurements considering residence time distribution (RTD) data. The results revealed that inside the reactor the bubble size distribution was uniform, and the flow was fully developed and independent of the inlet conditions. This observation indicates that a uniform distribution of bubble size can be presumed for modeling bubbly flow using CFD.

Similarly, CFD studies have been performed to predict two-phase flow characteristics in small diameter pipes at different inclination angles (0 – 90°). In 2008, Hernandez Perez employed CFD techniques to study the hydrodynamics of two-phase slug flow in small inclined pipes. To assess the accuracy of the model, simulation results including phase distribution, velocity field, and pressure drop were compared with experimental measurements. The model flow geometry consisted of 1.5 in (38 mm) internal diameter pipe and 6 m long. Two different pipe inclination angles were simulated: horizontal pipe and 45 degrees. A mixture of air and liquid water was selected as two-phase fluid. The flow was considered as isothermal and incompressible. The VOF approach model was chosen to model and capture the characteristics of two-phase slug flow. The simulation was carried out using FLUENT 6.1. The CFD model was able to demonstrate flow development along the pipe. Generally, the comparative study displayed a good quantitative agreement between simulation modeling results and experimental data. Da Riva and Del Col (2009) developed CFD simulation by employing VOF model to simulate churn flow in small diameter pipes up to 1.25 inches and superficial gas velocities of up to 19.7 ft/s. Their qualitative comparison of CFD predictions with experimental data showed an acceptable agreement. This result reveals the capability of VOF model in describing the churn flow characteristics.

Abulkadir et al. (2015) experimentally investigated two-phase slug flow in a vertical riser. Experiments were conducted using a test setup, which consisted of 6 m long vertical section and 2.6 in inner diameter. A mixture of air and silicone oil was used as the test fluid. They used liquid and gas superficial velocities of 0.05 and 0.344 m/s (0.164 and 1.129 ft/s), respectively. Along with their experimental work, they constructed two-phase flow simulation model to investigate the potential application of the models. A VOF two-phase flow approach was implemented using a commercial CFD codes Star-CD and Star-CCM+. The CFD model was aimed to simulate and characterize the observed slug flow regimes (e.g. void fraction in liquid slug and Taylor bubble, lengths of liquid slug and Taylor bubble, slug frequency, structure velocity). The results of their model were qualitatively and quantitatively validated with the experimental data. An acceptable agreement between the measured and predicted gas void fractions at various axial locations along the pipe was found.

To assess the capability of CFD based multiphase flow models on accurately predicting complex flow pattern such as churn flow, Parsi et al. (2015) studied churn and annular flows in a 3-in ID pipe. The simulated test section consisted of 3 m long vertical section and 1.9 m horizontal

section. A hybrid approach (combination of VOF and Eulerian model) of multiphase flow model was employed to simulate high-velocity air-water multiphase flow in vertical pipe. In the simulations, the inlet velocity conditions was varied from 10.3 to 33.9 m/s and two liquid superficial velocities (0.3 and 0.79 m/s) were considered. To validate their model predictions, they compared predicted void fraction with experimental measurements obtained from Wire Mesh sensor (WMS). A good agreement between model predictions and measured data was reported with a maximum discrepancy of 9%. Hernandez-Perez et al. (2011) investigated the grid generation issues (particularly element type and structure of mesh) in the 3D simulation of two-phase air-water flow in pipe using CFD. The simulated test section was 3 in (0.076 m) inner diameter and 6 m long vertical pipe.

CFD is also employed to simulate fundamental processes involving bubble dynamics. In the study of bubble dynamics, the understanding of the behavior of a bubble rising through a liquid is a complex phenomenon. Lun et al. (1996) carried out modeling of two-phase flow using a commercial CFD package. The study aimed to highlight the importance of adopting sufficient grid density for modeling wave in two-phase flow. The VOF technique was employed to model the motion, the shape and the size of bubbles as well as the motion of liquid phase. They commended the capability of CFD in simulating two-phase flow features. Due to the importance of determining the velocity of bubbles for pressure drop calculation in inclined intermittent gas-liquid flow, a numerical investigation was conducted by Cook and Behnia (2001) using VOF model. The study was aimed to investigate the drift of bubbles in stagnant liquid. The predicted bubble interface shape was compared with measurements obtained from a parallel wire conductance probe. The model predictions reveal that VOF method is able to simulate interface of bubbles rising in a quiescent liquid remarkably well. A summary of the literature survey on multiphase flow modeling using CFD is presented in Table 3.1.

Table 3.1 Summary of the literature survey on modeling of multiphase flow using CFD

Reference	Simulated test section	Test velocity (m/s)	Simulated flow pattern	Multiphase model	Remarks
Zabaras et al. (2013)	ID = 11-in L = 40 ft	NA	Bubble, churn, churn/semi-annular, and semi-annular flow	- Transient volume of fluid (VOF) model - Eulerian-Eulerian model	- CFD simulation was validated against their flow loop measurement and OLGA simulation - Good agreement between simulation results and experimental data
Waltrich et al. (2015)	ID = 1 – 12-in L = 20 – 50 ft	$V_g = 0.093 – 15.87$ $V_l = 0.050 – 1.100$	Dispersed bubble, bubble, agitated bubble, churn flow	- Volume of Fluid (VOF) model - Hybrid model - Mixture model	- CFD simulation model was validated against several existing experimental measurement and field data. - VOF model shows reasonable agreement with experimental data, especially at high slip ratio. - Hybrid model provides better accuracy at high slip ratio. However, it is difficult to stabilize. - Multiphase mixture model is less accurate comparing to VOF and Hybrid models.
Sanati (2015)	ID = 8-in L = 40 ft	$V_g = 0.03 – 4.7$ $V_l = 0.18 – 1.06$	Bubble and slug	- Mixture model	- Fair agreement was found between model predictions and measurement. - Flow pattern was predicted using existing empirical correlations.
Yancheshme et al. (2016)	ID = 19-in L = 11 ft	$V_g = 0.14$ $V_l = NA$	Churn flow	- Euler-Euler approach	- Simulation results are validated with their measurement in terms of residence time distribution (RTD) data. - Bubble size distribution inside reactor is fully developed and independent of the inlet conditions.
Hernandez Perez (2008)	ID = 1.5-in L = 11 ft	$V_g = 0.15 – 0.9$ $V_l = 0.1 – 0.7$	Slug flow	- Volume of Fluid (VOF) model	- The model results were validated with his own experimental data. - CFD simulation model was able to capture flow development along the pipe
Da Riva and Del Col (2009)	ID = 1.25-in L = NA	$V_g = 6$ $V_l = NA$	Churn flow	- Volume of Fluid (VOF) model	- Assure the capability of CFD-VOF model for predicting churn flow characteristics
Abulkadir et al. (2015)	ID = 2.6-in L = 20 ft	$V_g = 0.344$ $V_l = 0.05$	Slug flow	- Volume of Fluid (VOF) model	- Simulation model results were qualitatively and quantitatively validated with the experimental data. - Acceptable agreement between the measured and predicted was found.

Parsi et al. (2015)	ID = 3-in L = 9.8 ft	V_g = 10.3 – 33.9 V_l = 0.3 – 0.79	Churn and annular flow	- Hybrid model	- Good agreement between model predictions and measured data of the void fraction with a maximum discrepancy of 9%
Hernandez Perez et al. (2011)	ID = 3-in L = 19.7 ft	V_g = 0.15 V_l = NA	NA	- VOF model	- The study aimed at investigated the grid mesh generation issues in CFD modeling of two-phase flow in a pipe - Best model predictions were obtained with Butterfly and unstructured grids

3.2. CFD Modeling of Flow in Annulus

Past modeling works for vertical flows have been mostly focused on flow in pipe. The work in the area of flow in the annulus has been limited. The main difference between the CFD study of pipe flow and that of annular flow is the geometry which affects grid structure and the numerical approach. Pipe flow has single wall boundary where the velocity is zero, high turbulent dissipation rate, and minimum turbulent kinetic energy. However, in the case of annular flow, there are two walls: one at the outer face (casing wall) and the other at the inner face (tubing wall), as shown in the **Figure 3.1**. The change in geometry results in the variation of flow characteristics that causes a change in flow patterns, pressure gradient, and liquid holdup.
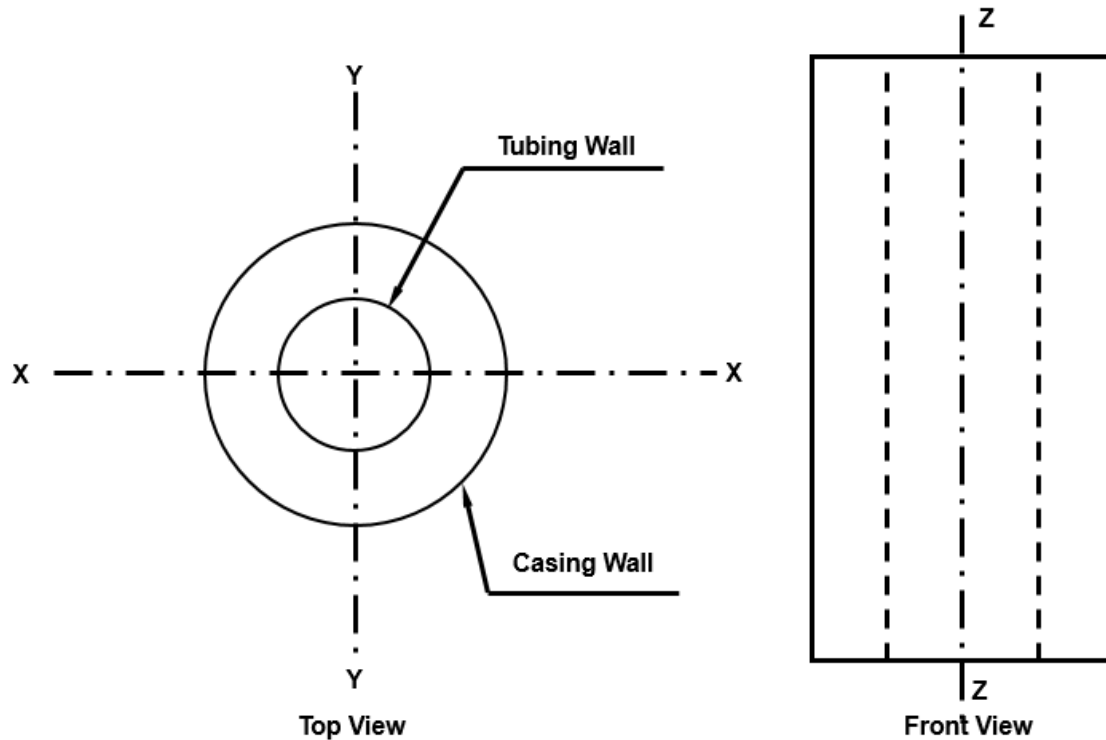
Figure 3.1 Geometry of annulus

Sorgun et al. (2013) studied two-phase (air and water) flow in horizontal annuli. The study encompassed the modeling of different flow patterns including dispersed bubbly, dispersed annular, plug, slug, and wavy annular flows using the mixture model in ANSYS CFX. In the study, the inhomogeneous model was used with interphase force transfer considering mixture model and free surface model in addition to the basic conservation equations. At the inlet, the velocities and volume fraction of different phases were specified while the pressure boundary condition was implemented at the outlet boundary. The superficial gas velocity ranged between 0.3 to 24 m/s while liquid velocity of 0.3-3 m/s was considered. In addition, the drag coefficient was assumed to be 0.44. The maximum error reported in the simulation result was 31.1%. It was

inferred that the pressure gradient would be higher for concentric annuli in comparison to fully eccentric annuli.

Majority of existing CFD studies related to multiphase fluid flow in small or large diameter pipes were conducted at relatively low Mach numbers (less than 0.3). There is a lack of experimental data for high Mach numbers (0.3 – 1.0 and above 1.0) two-phase flows. To have a better understanding of the physical process associated with turbulent multiphase flow throughout different flow geometries (pipe and annulus), a comparative study is carried out to validate our simulation predictions with existing measurements.

4. CFD Modelling

CFD modeling has become an inevitable part of multiphase flow investigation. It is often used to describe the flow characteristics and get insights into the flow pattern beforehand. In some applications such as worst case discharge, it is difficult to replicate real-field conditions at the laboratory scale and hence, the significance of CFD is more pronounced. In order to use CFD, it is necessary to validate and verify its predictions using experimental data and perform sensitivity analysis. Then, a CFD model can be applied to simulate the desired flow. In this study, the same strategy is adopted. First, CFD models are constructed and validated using published measurements. After that, CFD models for the current laboratory setup has been developed which will be further used to verify the model with the measurements obtained at high velocities. After performing extensive validation, the model will be used to simulate large diameter high-velocity two-phase flows in pipes and annuli. In addition, a strategy has been established to apply results of CFD modeling for WCD model development.

4.1 Modeling for Flow in Pipes

4.1.1 Validation of CFD Model LSU Data

Due to their completeness and extensiveness, experimental measurements reported by Waltrich at al. (2015) are selected for model validation purpose. Three sets of test measurements obtained from 2, 8 and 12 in pipe diameters are chosen. The modeled test sections consisted of 20.6, 36, and 23.4 ft long, respectively. **Figure 4.1** presents a schematic of the test sections. In this simulation, VOF approach with k-ε turbulent model is employed. The details of CFD simulation are presented in the following sections.

4.1.1.1 Mesh Sensitivity Analysis

To carry out the simulation, a commercial CFD package ANSYS 18.1 was used. For 2-in measurement, the flow map developed by Waltrich et al. (2015) suggests that various flow patterns including bubble, slug and annular flow can be observed. On the other hand, most of the 8-in data selected for simulation validation indicates the establishment of bubbly or agitated bubbly flow. A number of CFD studies (Zabaras et al., 2013; Parsi et al., 2015; Hernandez-Perez, 2008; Hernandez-Perez et al., 2011; and Abdulkadir et al., 2015) confirmed the usefulness of the VOF multiphase model in simulating different flow patterns including bubbly, agitated bubbly, and slug flow in the vertical pipe.

Mesh size optimization is very critical for CFD modeling. Large grids result in low resolution and inaccuracy. Fine grids create instability and increase computational time. To identify the minimum mesh density that is required for the solution to be independent of mesh resolution, a sensitivity analysis has been conducted. The analysis was performed for 2, 8 and 12 in inner diameter pipes. The mesh sensitivity analysis for 8-in pipe is presented in Section 4.2.1 along with experimental data reported by Ohnuki and Akimoto (2000). In the present CFD simulations, a computational domain length of 2 m was selected as a sufficient length to simulate two-phase flow characteristics for an incompressible fluid. This assumption was found consistent with

existing two-phase flow CFD models (Hernandez-Perez, 2008 and Abdulkadir et al., 2015). For 2-in pipe diameter, four grid sizes: a) 22K; b) 43K; c) 80K and d) 223K were tested during the analysis. **Table 4.1** lists details of the grids used in this analysis.. Similar grid analysis was performed for 12-in simulated pip and e test section, and 99K grid size was optimized to carry out the simulations. A reasonable matching between simulation prediction and experimental data was found at a grid size of 43K. Afterward, all the model simulations of 2-in pipe diameter were carried out using the optimum grid size of 43K. The results of grid size analysis for 2-in pipe diameter are shown in **Figure 4.3**.
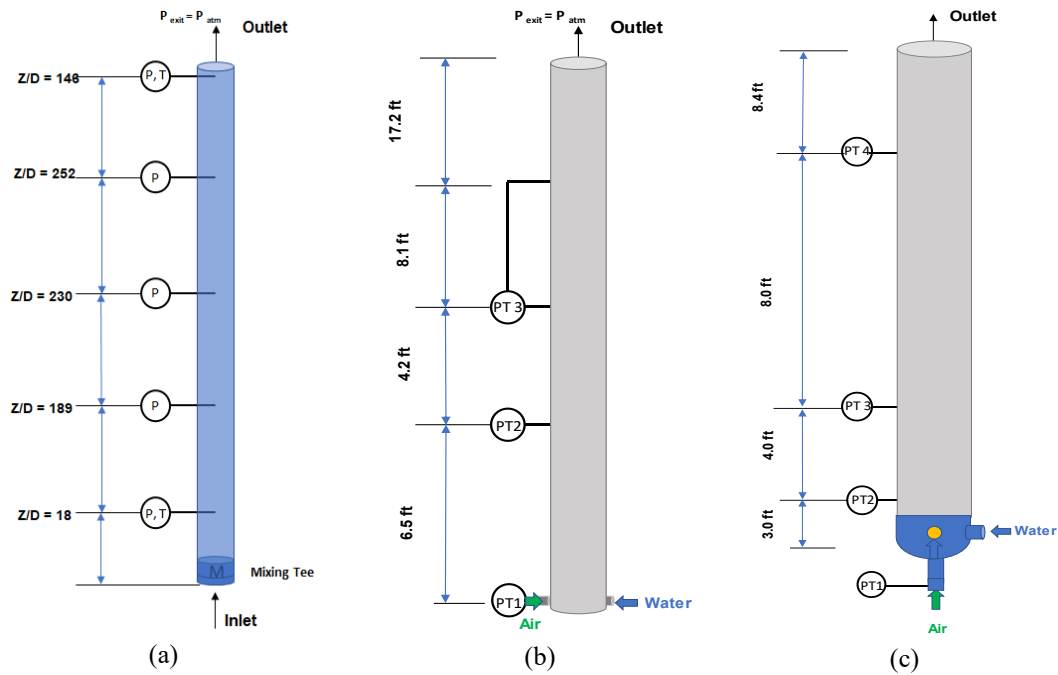

(a)   (b)   (c)

Figure 4.1 Schematic of experimental setups used to validate CFD study: a) 2-in; b) 8-in; and c) 12-in (Waltrich et al., 2015)
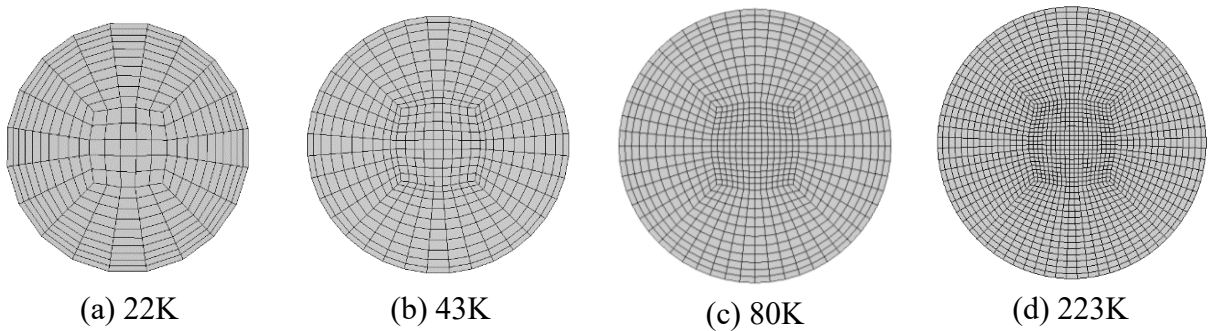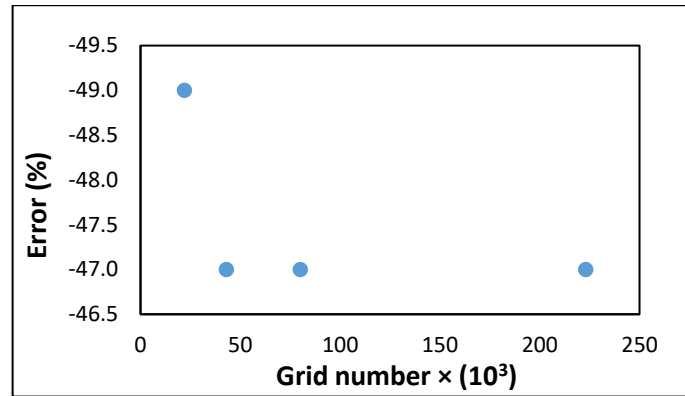

(a) 22K   (b) 43K   (c) 80K   (d) 223K

Figure 4.2 Grids and their topology used to validate CFD models against 2-in experimental data

Table 4.1 Number of cells used in different Grids

Grid name	cross-section	Total number of cells	Maximum aspect ratio
Type (a)	225	22275	21
Type (b)	441	43659	23
Type (c)	812	80388	22
Type (d)	1501	223649	21

Figure 4.3 Results of grid sensitivity analysis for 2-in pipe

4.1.1.2 CFD Solver Setup

Three-dimensional transient simulations were performed using pressure-based solver to reproduce experimentally measured pressure gradient reported by Waltrich et al. (2015). The effect of the gravity was considered in the flow direction. The standard operating pressure and density were defined as 101.325 KPa and zero, respectively. In addition, it was presumed that both simulated phases (air and water) were incompressible, and no mass transfer was considered between the two phases. The flow was assumed to be an adiabatic and no-slip condition at the wall. The roughness height was given a value of 0.0006 (Waltrich et al., 2015). For multiphase flow model, VOF implicit approach with dispersed phase interference modeling was selected. Among the turbulent models available in ANSYS 18.1, the realizable k–ε model with scalable wall function and the default setting of the model constants was employed to model the turbulent in the continuous phase. In all simulations, the air was specified as primary phase, and liquid water was selected as a secondary phase. The phase interaction force between the two phases was considered by activating surface tension feature and set its coefficient at 72 dyne/cm. Besides, various options were selected for solving CFD model. The Pressure-Implicit with Splitting of Operators (PISO) method with skewness and neighbor correction of 1 was used for pressure-velocity coupling scheme. Concerning the spatial discretization, the following options were selected: PRESTO (PREssure STaggering Option) pressure discretization; density second order upwind; momentum third order MUSCL (Monotonic Upwind Scheme for Conservation Laws); volume faction first order upwind with bounded second order implicit transient formulation; turbulent kinetic energy and dissipation rate are first-order upwind. In order to obtain a converged solution, the following under-relaxation factors were considered: 0.19 for

pressure; 1 for density; 1 for body force; 0.37 for momentum; 0.5 for volume fraction; 0.8 for turbulent kinetic energy and dissipation rate; and 0.53 for turbulent viscosity.

CFD simulation model has three boundary conditions, inlet, outlet and wall boundary conditions. At the inlet pipe boundary condition, fixed mass flow inlet was employed for both air and water. On the other hand, a pressure outlet boundary condition was implemented at the exit of the pipe and set it to zero static pressure. No-slip boundary condition was specified at the wall.

As the initial conditions, the entire domain was assumed to be filled with liquid phase at zero initial velocity (air volume fraction is equal to zero). In all simulations, the time step and a maximum number of iterations per time-step were selected to be 0.001 seconds and 20, respectively. After testing different values of residuals, the maximum residual was set at 0.001. To attain the steady state flow condition, all the simulations were carried out at least for 3 s, which corresponds to 3000-time steps.

4.1.1.3 Results

A wide range of gas and liquid superficial velocities were used in this simulation to reproduce experimentally measured (Waltrich et al. (2015) pressure gradient. The results are compared in **Table 4.2**. The predicted pressure gradient is obtained considering 2 m long pipe sections. A reasonable agreement between CFD simulation results and experimental measurements was found. The discrepancy between simulated and measured pressure loss could be attributed to the error in the test measurement and failure of VOF approach of capturing flow characteristics at high slip ratio.

Table 4.2 Comparison of CFD model predictions with Waltrich's experimental data

Case	Pipe diameter (in)	V_{SG} (m/s)	V_{SL} (m/s)	CFD (DP/DL) (Pa/m)	Exp. (DP/DL) (Pa/m)	Error (%)
1	2	1.20	0.30	2126	4072	-47
2	2	5.79	0.30	1380	2488	-45
3	2	11.58	0.30	1855	2036	-8
4	2	18.29	0.30	2714	2036	34
5	2	1.23	0.13	1131	3167	-67
6	2	6.68	0.13	679	1945	-68
7	2	12.83	0.13	950	1470	-34
8	2	18.29	0.13	1267	1244	0.77
9	2	23.77	0.13	1629	1108	49
10	8	0.973	0.43	3506	5881	-41
11	8	5.58	0.43	927	2398	-61
12	8	7.07	0.43	950	2172	-56
13	8	13.11	0.43	860	1583	-46
14	12	1.12	0.46	3167	6266	-49
15	12	6.68	0.46	1448	3280	-55
16	12	7.68	0.46	1289	2285	-40

To interpret CFD simulation results, a sample of the predicted static pressure profile along the test section at superficial liquid velocity 1 ft/s (0.3048 m/s) and two superficial gas velocities (1.20 m/s and 5.79 m/s) is presented in **Figure 4.4**. As anticipated, pressure declining was observed with the length of the test section, reaching its minimum value at the outlet. Under a particular simulation condition, the pressure gradient was almost constant along the test section. The pressure gradient was considerably decreased with superficial gas velocity, which is expected trend due to a reduction in the hydrostatic component of the total pressure drop. Increasing the gas velocity tends to drag the liquid phase to travel with same speed and consequently results in the low liquid holdup. Thus, it reduces the hydrostatic pressure. In addition, the effect of test section entrance on pressure profile was clearly observed at high gas superficial velocity (green line), as shown in Figure 4.4.
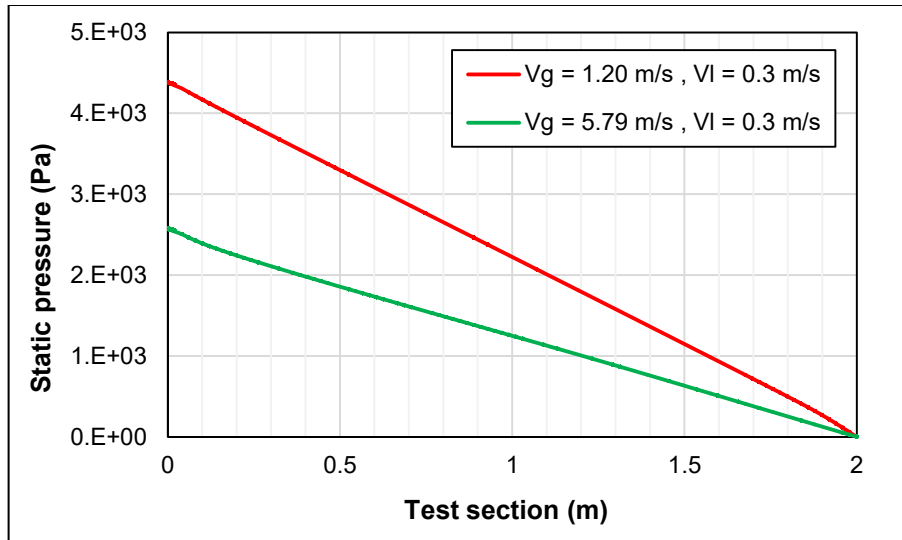
Figure 4.4 Pressure profile of the simulated flow geometry (2-in pipe) at 0.30 m/s liquid velocity and two different superficial gas velocities (1.20 m/s and 5.79 m/s)

Besides the pressure profile, cross-section mixture velocity, turbulent kinetic energy, and turbulent dissipation rate profiles are presented in **Figures 4.5** and **4.6**. These profiles were developed in 2-in pipe diameter at 1.20 m/s and 0.30 m/s of superficial gas and liquid velocities, respectively. As displayed in Figure 4.5, a typical cross-section velocity profile is obtained where it has a maximum value at the core of the pipe and zero at the wall. It is also indicated that the flow is approximately established near the inlet and has a fully developed profile at 0.2 near the outlet. This observation reveals the strength of the assumption that proposes 2 m for modeling test section as a sufficient length for the fully developed flow. Based on Reynolds number calculation (Re = 4148), the flow under these conditions can be classified as transient or low Reynold number turbulent flow. This finding has been consistent with CFD simulation predictions of turbulent kinetic energy and dissipation rate, as depicted in Figure 4.6. It can be seen that the intensity of k and ε are very low at the core of the pipe, which are in the range of 10-2 m^2/s^2.
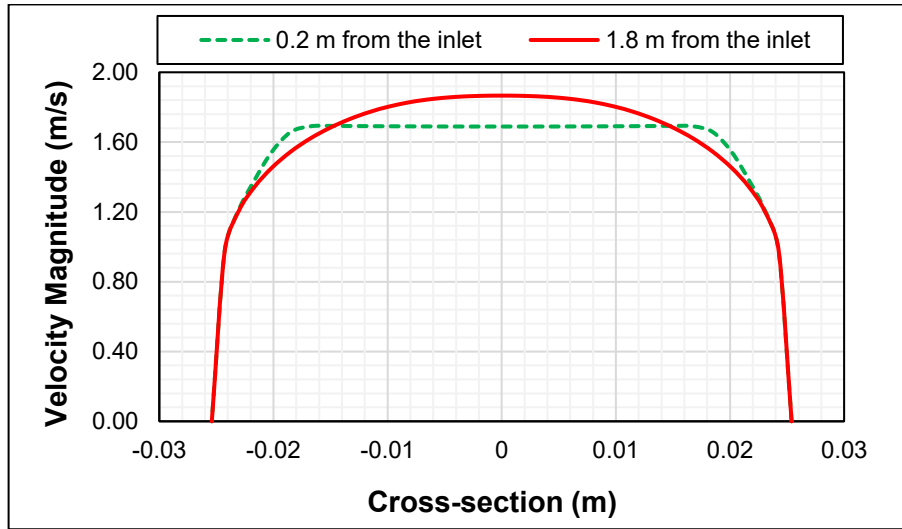
Figure 4.5 Cross-section predicted mixture velocity profile for 2-in pipe at different locations from the inlet (0.2 and 1.8 m)

| (a) | (b) |
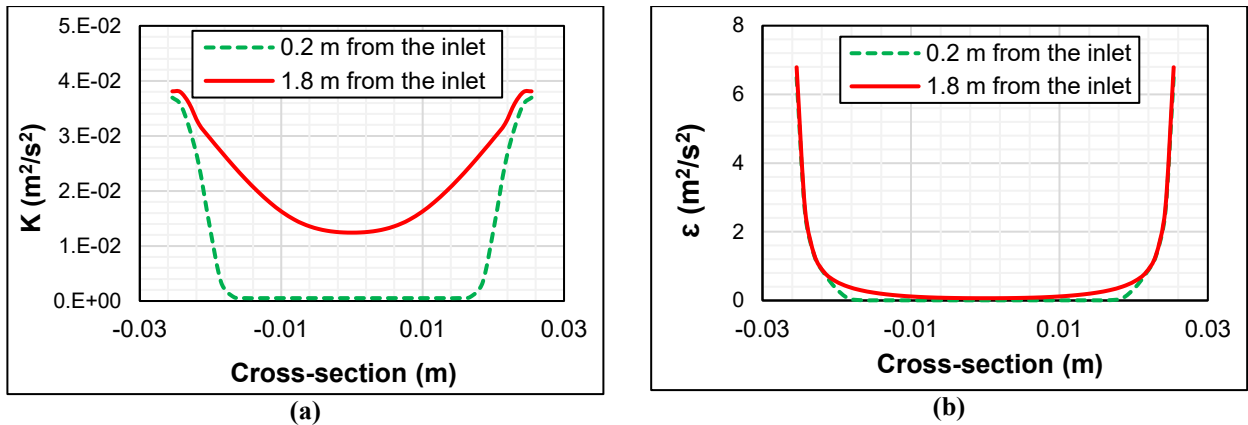
Figure 4.6 Turbulent flow characteristics at two different locations from the inlet (0.2 and 1.8 m) of 2-in pipe: a) Turbulent kinetic energy; b) Turbulent dissipation rate

4.1.2 Validation of CFD Model with Other Data (Ohnuki and Akimoto, 2000)

The Ohnuki and Akimoto (2000) experimental setup consisted of 8 in (0.2 m) inner diameter and 12.3 m total length of the pipe. The geometric details of the test section are shown in **Figure 4.7**. Four sets of data were selected at different gas and superficial water velocities to validate the simulation model results. Using existing empirical correlations (Duns and Ros, 1963; Orkiszewski, 1967; Hasan and Kabir, 1988; 1990; Mukherjee and Brill, 1985), Sanati (2015) predicted the flow pattern for the experiments reported by Ohnuki and Akimoto (2000). At low superficial gas and liquid velocities (V_g between 0.03 and 4.17 m/s, and V_l between 0.18 and 1.06 m/s), the flow characteristic was identified as bubbly or slug flow.

4.1.2.1 Mesh Sensitivity Analysis

Prior to carrying out the simulation, a mesh sensitivity analysis (Grid-independent test) was carried out. The main goal of this analysis is to verify the minimum grid resolution required to develop a solution, which is independent of the grid size and topology used. A 2-meter long computational domain was considered to simulate test setup (12.3 m long) developed by Ohnuki and Akimoto (2000). The model flow geometry was built and meshed using ICEM software and then imported to ANSYS 18.1, where the simulation and post-processing of the results were performed.

A group of CFD studies (Hernandez-Perez et al., 2011; Hernandez-Perez, 2008; Lo and Zhang, 2009) proposed the butterfly grid (O-grid) as the best type of mesh to simulate pipe flow geometry. The mesh sensitivity analysis was carried out reproducing the first data points by employing four grid sizes of (a) 29K; (b) 43K; (c) 80K; (c) 114K; and (d) 201K. **Figure 4.8** presented tested grid topology of these four grid sizes. Details of the grids employed in the mesh sensitivity analysis are shown in **Table 4.3**. An unstable solution was obtained in the case of 29K grid size. Thus, it was eliminated from the grid analysis study. The results of grid independence study are shown in **Figure 4.9**. Relatively high discrepancy (-48% error) between measured and predicted pressure drop with the lowest and the highest number of tested grid sizes. This error is attributed to relatively large grid size near the wall for case (a) and very fine grid size near the wall for case (c). In addition, for mesh type (d), the discrepancy is due to high maximum aspect ratio, which is roughly 100. A reasonable match between CFD simulation results and experimental data were obtained with grid size and topology of (b) and (c). Therefore, to minimize the computational time, 80K grid size was selected for the CFD simulations.
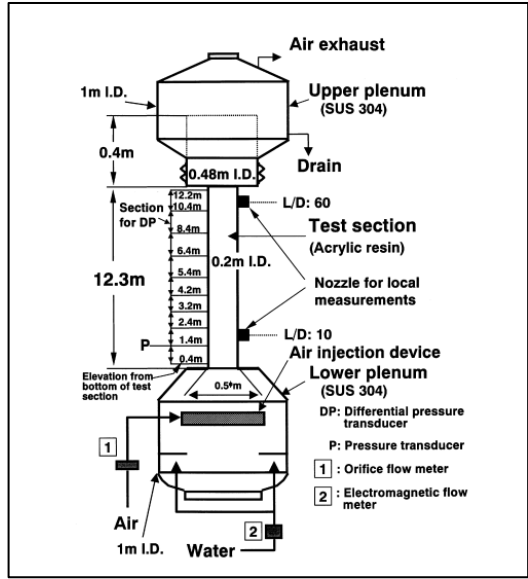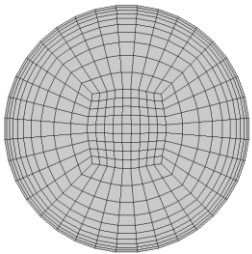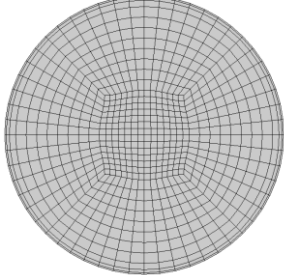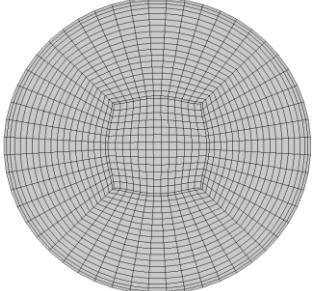
Figure 4.7 Schematic of test setup and DP transducer locations used for multiphase flow experiments (Ohnuki and Akimoto, 2000)
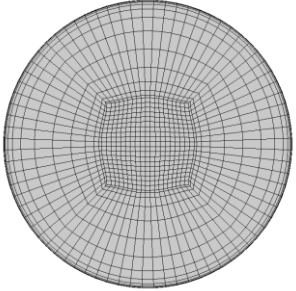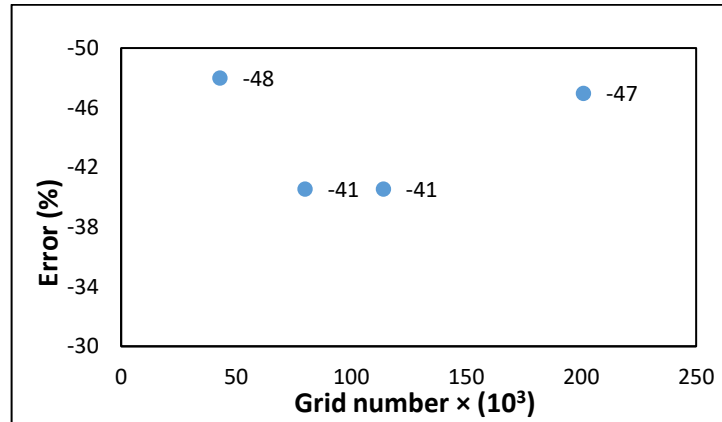

(a) 43K   (b) 80K   (c) 114K

(d) 201K

Figure 4.8 Four grids and their topology: a) 43K; b) 80K; c) 114K; and d) 201K used to validate CFD simulations against 8-in experimental data (Ohnuki and Akimoto, 2000 and Waltrich et al., 2015)

Table 4.3 Number of cells used in different Grids

Grid name	cross-section	Total number of cells	Maximum aspect ratio
Type (a)	441	43659	17
Type (b)	812	80388	22
Type (c)	1157	114543	16
Type (d)	1349	201001	103

Figure 4.9 Results of grid sensitivity analysis for 8-in pipe using four different grid sizes: a) 43K; b) 80K; c) 114K; and d) 201K

4.1.2.2 Results

In this comparative study, CFD solver was implemented to predict the pressure gradient using the same solution algorithm that was applied in Section 4.1.2. Four experimental data points were selected for CFD-VOF model validation. In addition, the CFD model predictions were compared to existing two-phase flow model developed by Sanati (2015). In the model, a mixture multiphase approach was employed for predicting pressure gradient across the simulated test section. Employing existing empirical correlations, Sanati (2015) classified the flow in the modeled test section as bubbly flow under the selected conditions of superficial gas and liquid velocities (Table 2). Simulation results were compared with available experimental and modeling data presented in **Table 4.4**.

As displayed from the comparative study, CFD simulation results exhibit good agreement with experimental data in which the maximum discrepancy of -40% was observed. Overall, it is indicated that Sanati's model slightly overpredicts the pressure drop, which will result eventually in underestimation of the worst case discharge rate. Moreover, the results reveal the capability of CFD-VOF model to predict characteristics of bubbly multiphase flows in vertical pipe. The predicted cross-section mixture velocity profile in the pipe for Case 2 ($V_g = 0.03$ and $V_l = 1.06$ m/s) at two different heights from the inlet is presented in **Figure 4.10**.
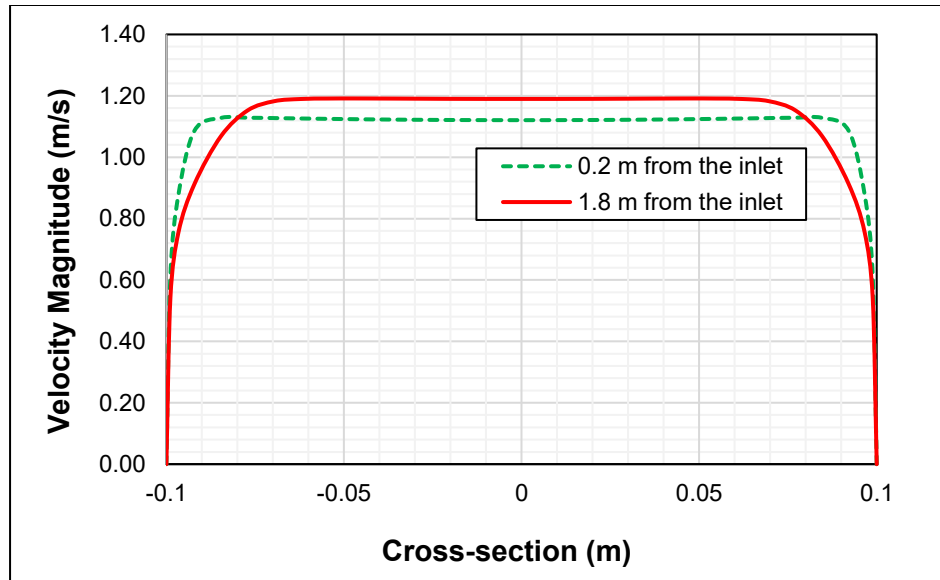
Figure 4.10 Cross-section mixture velocity profile for 8-in pipe at different locations from the inlet (0.2 and 1.8 m)

The plateau part of the velocity profile at mid-section of the pipe reveals that a fully turbulent flow is established. Typical profiles of turbulent kinetic energy and dissipation rate are shown in **Figure 4.11**. The common trend of turbulent kinetic energy is zero at the wall and then sharply increases to its maximum value with small distance from the wall. Afterward, it gradually declines till reaches its local minimum value at the center of the pipe (**Figure 4.11a**). Due to insufficient finer grids at the wall, CFD simulation was not able to capture the turbulent kinetic energy data point at the wall. **Figure 4.11b** shows a cross-section profile of the turbulent dissipation rate where it has a maximum value at the wall and minimum value, roughly zero, at the core zone.
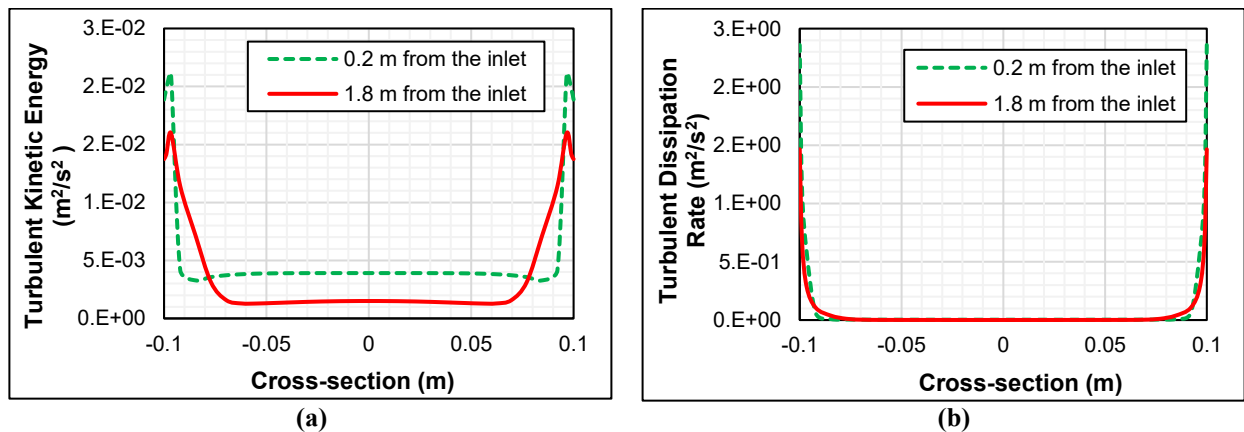
Figure 4.11 Turbulent flow characteristics: a) turbulent kinetic energy; b) turbulent dissipation rate at two different locations from the inlet (0.2 and 1.8 m) for 8-in pipe

Figure 4.12 displays the pressure profile along the modeled test section (ID = 8-in and L = 2 m) at a liquid velocity of 1.06 m/s and two different superficial gas velocities (V_g = 0.03 and 0.26 m/s). In general, the simulation results demonstrated an anticipated pressure profile in which the pressure is constantly decreasing along the length of the test section, reaching its minimum value at the outlet (P = zero at L = 2 m). Additionally, the results show a significant change in pressure gradient with superficial gas velocity. As expected, the pressure gradient considerably reduced as the additional amount of air was introduced into the test section. This observation indicates that the total pressure loss is dominated by the hydrostatic component of the total pressure drop rather than friction and acceleration.

Table 4.4 Comparison of CFD model predictions with experimental data (Ohnuki and Akimoto, 2000)

Case	Flow pattern	Pipe diameter (in)	V_{SG} (m/s)	V_{SL} (m/s)	CFD (DP/DL) (KPa/m)	Exp. (DP/DL) (KPa/m)	Existing model (DP/DL) (KPa/m)	Error (%)
1	bubble	8	0.03	0.18	9.50	9.05	9.43	5
2	bubble	8	0.03	1.06	9.65	9.7	9.5	0.5
3	bubble	8	0.26	0.18	4.22	7	NA*	-40
4	bubble	8	0.26	1.06	8.05	8.5	8.9	-5

NA: refers to non-available data.
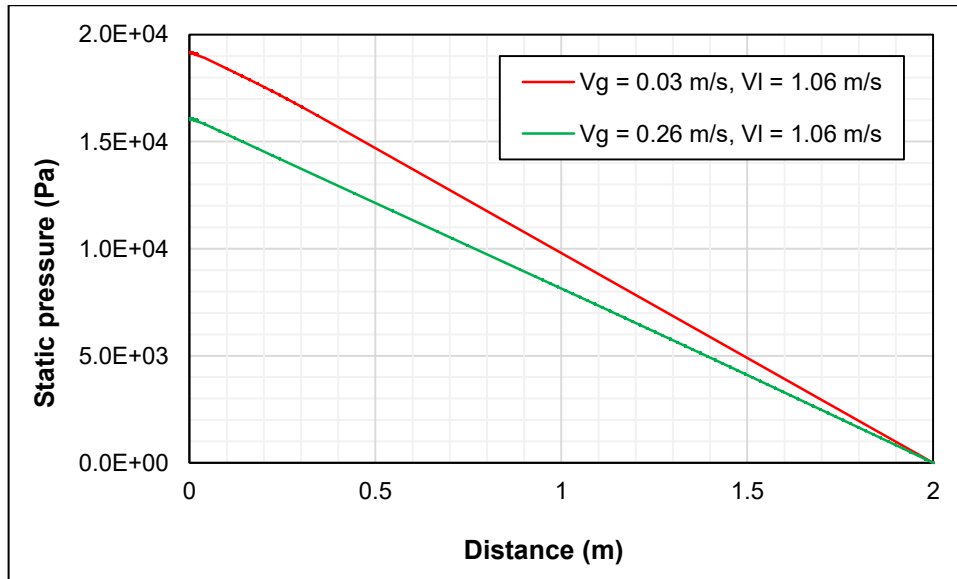
Figure 4.12 Pressure profile of the simulated flow geometry (2-in pipe) at 1.06 m/s liquid velocity

4.2 Model for Flow in Annulus

The flow in the annulus is one of the highly discussed area of multiphase flows considered in drilling operations. Most of the time, the drill pipe is present in the annulus while drilling. This makes the presence of flow in annulus a likely scenario during the worst case discharge. Therefore, the understanding of flow characteristics of two-phase flow in the annulus is of paramount importance. Keeping this in mind, a thorough simulation work was conducted for fluid flow in the annulus. The study encompassed construction of the geometry, meshing of the

flow domain, setting up the theoretical model, and solving the model in ANSYS Fluent. The geometry of the model is constructed using the geometry module of ANSYS and standard meshing option was used to obtain the desired grid structures. A sensitivity analysis was carried out to optimize the number of elements required for the simulation. After obtaining the optimum grid distribution system, several modeling options, such as Volume of Fluid and Eulerian, were tried to replicate the experimental results. Ultimately the most suited theoretical models and parameters were chosen to simulate the flow behavior in the annulus.

4.2.1 Mesh Sensitivity Analysis

For the mesh sensitivity analysis, one experimental data point was selected from available literature (Caetano, 1985). We used .048 m/s superficial gas velocity and 1.984 m/s superficial liquid velocity in the simulations with dispersed bubble flow pattern in air-water as two phases. Since the geometry of the flow domain is symmetric in nature, only one-fourth of the cross-section (shown by grid filled section in **Figure 4.13**) can represent the flow characteristics. The topology of the annular cross section is bounded by four edges. Hence, the uniform grid distribution was adopted. This hypothesis was validated by matching the results of the quarter domain with full annulus section.
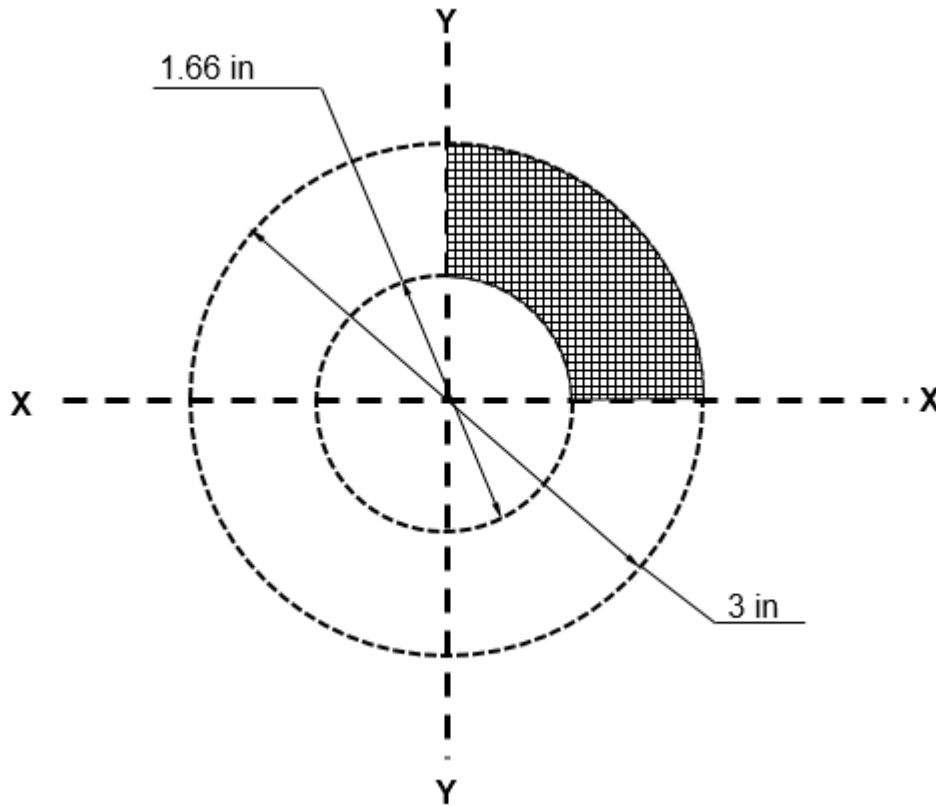
Figure 4.13 Cross-sectional area of the annulus

Past studies suggest that the flow is fully developed in the axial direction with the vertical height as 30-40 times the hydraulic diameter (Lien et al., 2004; Laufer, 1952; and Nikuradse, 1933). Therefore, only 2 m vertical height is considered for simulation of the annulus with the hydraulic diameter of 40 mm. The details of the study methodology are presented in Section 4.2.2. The variation of grid distribution was based on the number of nodes on the edges. **Figure 4.14** represents the typical grid distribution along the horizontal cross-section.
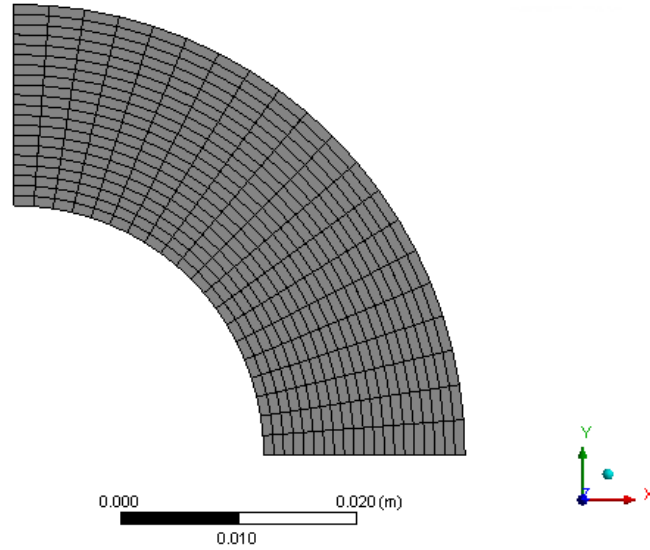
Figure 4.14 Uniform type grid distribution

Five set of variations in grid sizes were considered for sensitivity analysis as described in **Table 4.5**. Type 1 considers 300 elements (15 X 20) in the horizontal cross-section with 100 divisions in vertical direction. In this type of mesh, A and B are 15 and 20 divisions respectively. A and B respectively refer to a number of divisions along the edges corresponding to the plane of symmetry and number of divisions along the peripheral edge. Similarly, other types of meshes were also chosen.

Table 4.5 Number of elements used in different Grids

	Number of elements in cross-section (AXB)	Total number of elements
Type 1	300 (15 X 20)	30000
Type 2	400 (20 X 20)	40000
Type 3	500 (20 X 25)	50000
Type 4	500 (25 X 20)	50000
Type 5	400 (20 X 20)	80000

45

The simulation set-up was constructed using VOF implicit model with specified mass flow rate for both phases at the inlet and pressure boundary conditions at the outlet. It must be noted that since the quarter of the cross-section is used, one-fourth of the total mass flow rates should be used for both phases at the inlet. The walls of the tubing and casing were considered stationary with no-slip conditions. In addition, both the planes of symmetry were identified by symmetry boundary condition in ANSYS Fluent. **Table 4.6** and **Figure 4.15** depict the results for mesh sensitivity analysis. Results suggest that the Types 2, 3, 4, and 5 have comparable errors. It can be inferred that the error increases with the aspect ratio especially for the elements in the horizontal plane. Type 2 and 3 have error difference of 0.02%. Since the number of grids are less in case of Type 2, it is used for simulation of the low velocities. It is also worth mentioning that the grid sensitivity analysis only gives an idea about the significance of mesh quality with respect to the input parameters. In this case, it can be inferred that Type 2 grid was the best fit. However, it was later observed that this type of mesh led to convergence issues for high velocity and hence, the number of grids was increased. Type 5 mesh was found to be more suitable for high-velocity case, and it can be attributed to its low aspect ratio.

Table 4.6 Mesh sensitivity results for Cateano's experimental result

	Experimental Pressure Gradient (Pa/m)	Pressure Gradient (Pa/m)	Error (%age)	Maximum aspect ratio in vertical direction	Aspect ratio in horizontal direction
Type 1	9847	11597	+17.4 %	17.66	2.99
Type 2	9847	11535	-4.92 %	23.55	2.36
Type 3	9847	9385	-4.94 %	23.54	2.35
Type 4	9847	9374	-5.05 %	29.43	4.36
Type 5	9847	9385	-4.91 %	11.77	2.36
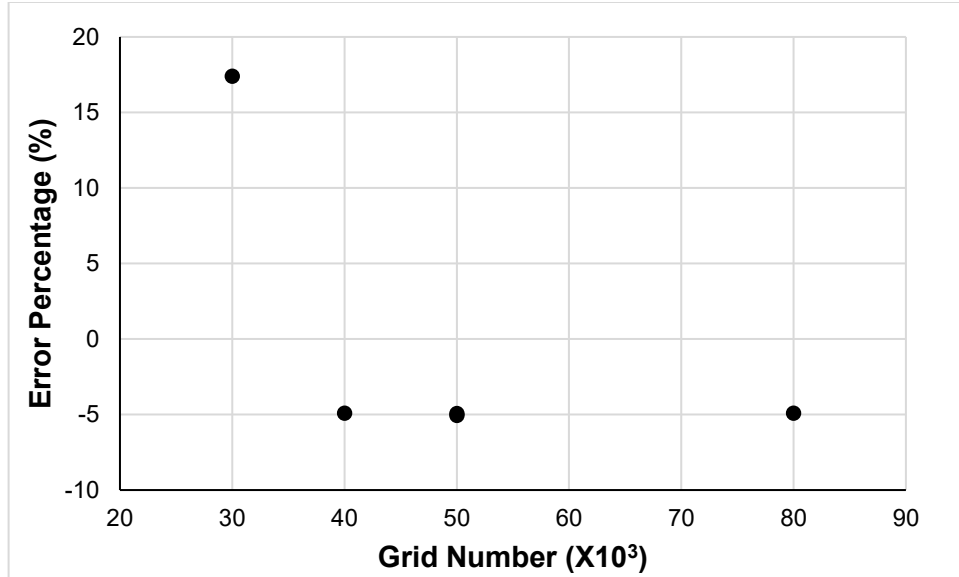
Figure 4.15 Results of CFD grid independence study for flow in the annulus - number of grid vs. error percentage for simulated pressure drop with respect to experimental pressure drop (Caetano's dataset)

Another sensitivity analysis was conducted for different types of mesh distributions. In the previous case, all the mesh sizes were uniform in radial and tangential direction. In the next sensitivity analysis, we used non-uniform grid sizes in the radial direction. From the previous sensitivity analysis, it was found out that Type 2 case was the best fit. Therefore, the size pattern in the radial direction was changed. At the walls, thin meshes were used to capture the boundary layer phenomenon. The new grid system is shown in **Figure 4.16**. In this case, a bias factor of 4 was used in the radial direction. The overall aspect ratio varied from 12.96 to 51.84 with the average of 28.53. The error observed, in this case, was 15.68%, which is attributed to high aspect ratio.

47

Figure 4.16 Non-uniform grid distribution

4.2.2 Validation of CFD with Caetano's Experimental Data

Two types of models were considered for simulation: (a) VOF implicit and (b) Eulerian model. In the VOF model, the transient case was simulated. At the dispersed phase interface, implicit body force, and surface tension were implemented in the model. The surf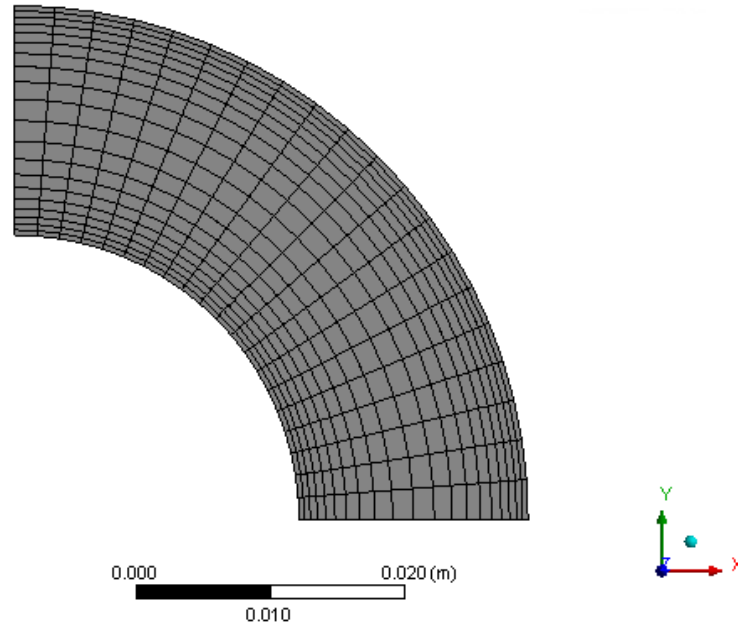ace tension between water and air was assumed to be constant at 0.072 N/m. Water and air were two phases. Both phases were considered to be incompressible in nature. The density of air and water was assumed to be 1.225 and 998.2 kg/m^3 respectively. The viscosity of air was 1.7894 X10^{-5} kg/m-s while for water it was 0.001003 kg/m-s. In the bubble flow pattern, water was assumed as the primary phase while in the slug, annular and churn flow patterns, air was considered as the primary phase. In addition, the k-ε realizable model was used to implement the effect of turbulence in the system. Since the effect of temperature and compressibility was neglected, the energy equation was not considered. However, the implicit body force was enacted in the model. In case of large body forces, the equilibrium condition exists between body force and pressure gradient terms of the momentum equation, as the contribution from convective and viscous terms are relatively negligible. In such cases, the convergence issue dominates when the partial equilibrium of pressure gradient and body forces is not considered. By implementation of implicit body force in Fluent, such problems are taken care off.

4.2.2.1 Boundary Conditions
The casing and tubing walls were assigned as the stationary boundary with the no-slip condition. The pipe roughness height was considered to be 0.0006, while the roughness constant was 0.5. The mass flow rate was imposed as inlet flow conditions for both phases. The initial gauge pressure was assumed to 0 Pa with the flow in axial direction. The turbulence was specified in

terms of intensity and hydraulic diameter. The intensity was assumed to 5%, while the hydraulic diameter was 0.034 m in this case. The hydraulic diameter is the difference between the inner and outer diameter of the annulus. The flow rates were specified based on the given velocity of both phases. In addition, both planes of symmetry were defined as symmetry condition in ANSYS Fluent. At the outlet, pressure boundary conditions were implemented. The outlet was open to atmosphere, and hence the pressure at the boundary was considered to be 0 Pa (gauge pressure). Also, the operating density was specified to be the density of the air, as the outlet was assumed to be in contact with air.

4.2.2.2 Solver Set-up

The pressure based segregated algorithm, Pressure-Implicit with Splitting of Operators (PISO) was enabled with 1 as skewness and neighbor correction factor. PRESTO (PREssure STaggering Option) for pressure, second-order upwind scheme for density, third order MUSCL (Monotone Upstream-Centered Schemes for Conservation Laws), second order upwind for volume fraction, first-order upwind for turbulent kinetic energy and dissipation rate was implemented. In addition, bounded second order implicit transient condition was imposed to minimize the variation in iterative solution. The models were tuned for different under-relaxation factors to reduce the divergence issues. Finally, a set of under-relaxation factors were adopted to optimize the computational effort as shown in Table 4.7.

Table 4.7 Under-relaxation factors and its values for simulation

Under-relaxation factors	Values
Pressure	0.3
Momentum	0.3
Density	1
Body forces	0.5
Turbulent kinetic energy	0.6
Turbulent dissipation rate	0.6

The standard initialization method was based on inlet flow conditions. After the initialization, the flow domain was patched for full water in the whole flow domain. The step size was 0.001s with 100 iterations allowed for each step to meet the convergence criteria. The standard convergence criteria of 0.001 was selected for residuals of continuity, velocity (u, v, w), kinetic energy (k) and dissipation rate (ε). Furthermore, several other parameters such as net mass flux, volumetric average pressure and void fraction were tracked with time-step. The monitoring of these additional parameters was essential to judge the full development of flow in the whole domain. It was inferred that the average pressure and water volume fraction stabilizes and attains approximately constant value in case of fully developed flow (shown in **Figures 4.17** and **4.18**). Also, the net mass flux rate achieves magnitude on the order of 10-10 or lower. A summary of CFD simulation results of air-water flow in the annulus is presented in **Table 4.8**. To illustrate the results, one case was chosen and presented here. The value of volumetric average pressure

stabilizes to a constant value which signifies the establishment of fully developed flow in the system. Also, the average value of water volume fraction stabilizes to constant value with time which again indicates the establishment of fully developed flow condition.
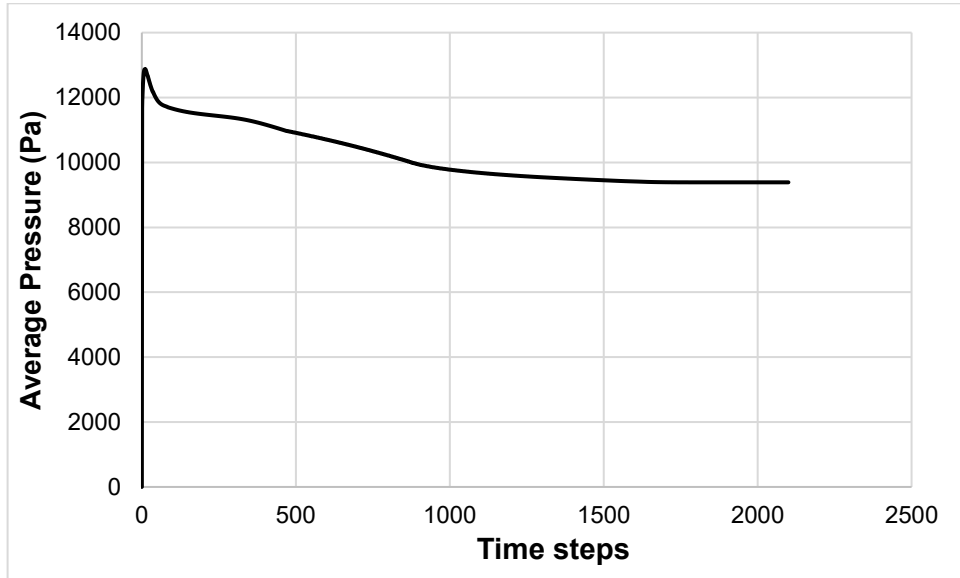
Figure 4.17 Average pressure in the test section with time steps
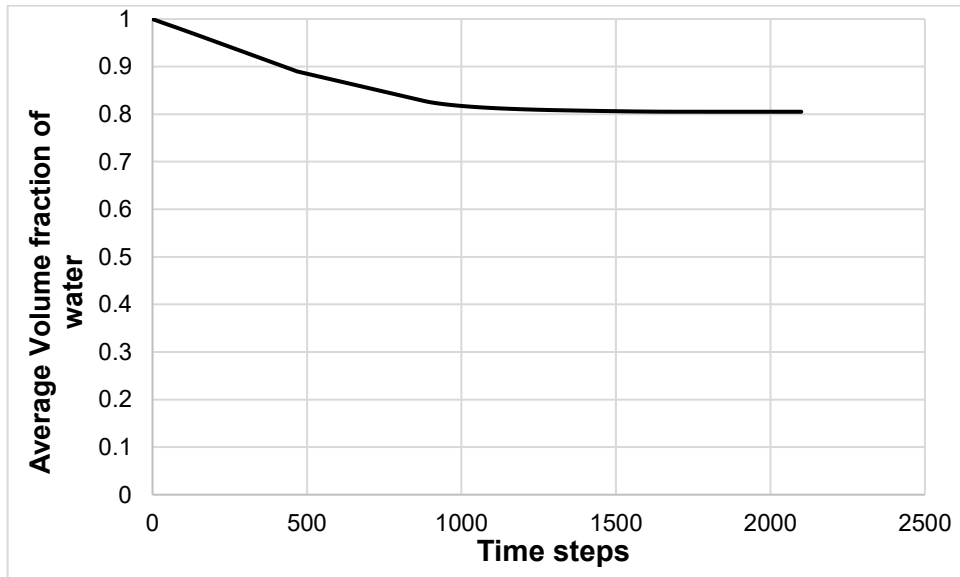
Figure 4.18 Volumetric average volume fraction of water with time steps

For experimental condition with superficial gas velocity of 0.48 m/s and liquid velocity of 1.984 m/s, the pressure gradient was 9876 Pa/m. Using the above specified simulation scheme, the pressure profile obtained from simulation is presented in **Figure 4.19**. The simulated pressure gradient was 9390.4 Pa/m which is within 5% discrepancy with the experimental measurement.
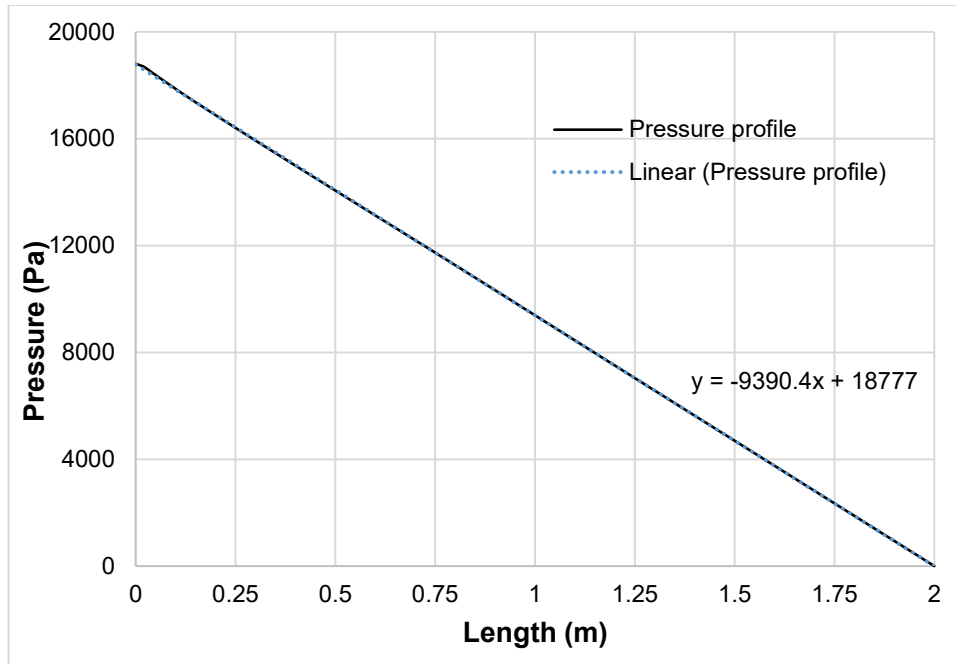
Figure 4.19 Linear pressure profile in the axial direction

The profiles of velocity, turbulent kinetic energy, and turbulent dissipation rate at different cross-sections are depicted in **Figures 4.20-4.22**. The velocity profile confirms that the velocity is highest in the mid-section while zero at the walls. Since the wall is considered stationary, the velocity of fluid should be zero in the vicinity of the wall. The opposite trend is observed for turbulent dissipation rate and it is common in pipe flow where very high turbulent dissipation rate is observed near the walls. However, if we look at the turbulent kinetic energy, it has some finite value which is contradictory to normal flow characteristics. It is a common practice to use the tradeoffs between accuracy and speed in CFD modeling. We believe, since the thickness of the grid structure used near the wall was not on the order of the desired condition to achieve the boundary layer effect, the simulation was unable to capture the boundary layer characteristics and consequently it shows finite turbulent kinetic energy at the wall.
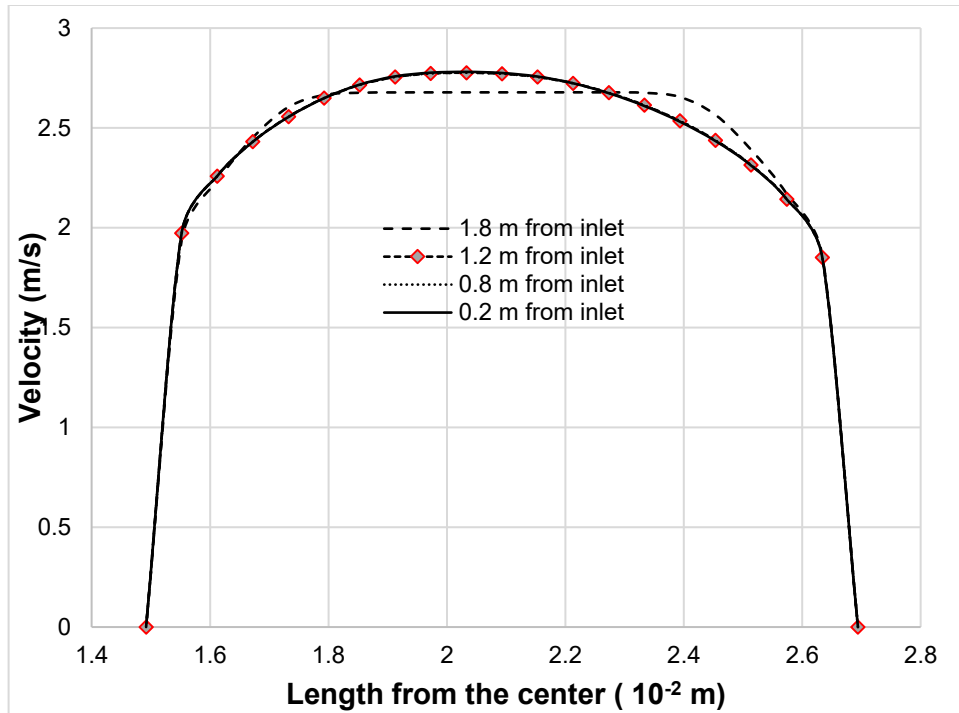
Figure 4.20 Velocity profile in the radial direction at a different height

Velocity is zero in the vicinity of casing and tubing wall (Figure 4.20) and displays the highest value in mid-section. Also, the velocity roughly displays a logarithmic profile near the outlet, which is expected. The turbulent kinetic energy (Figure 4.21) is high in the vicinity of the wall and minimizes in the core of the annulus. Also, it is the minimum at the inlet. The turbulent dissipation rate (Figure 4.22) is the highest along the wall and decreases to zero in the core of the annulus. Also, it is roughly constant with height.
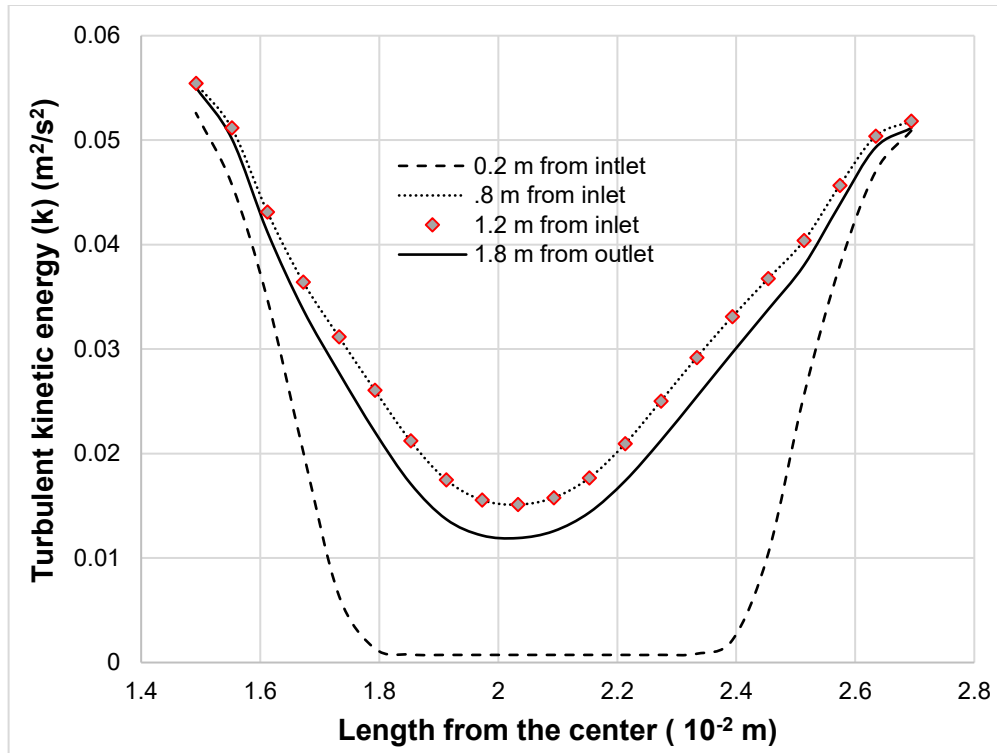
Figure 4.21 Change in turbulent kinetic energy in the radial direction

Figure 4.22 Change in turbulent dissipation rate in the radial direction

The summarized CFD simulation results (**Table 4.8**) show more substantial error in most of the cases of high slip-velocities. Also, it is worth mentioning, that the CFD simulated pressure drops are lower than the experimental ones. This comparatively small pressure drop makes it

conservative from the worst-case discharge calculation point of view. Caetano's modeling results suggested that in case of annular and slug flow, the pressure gradient calculated from t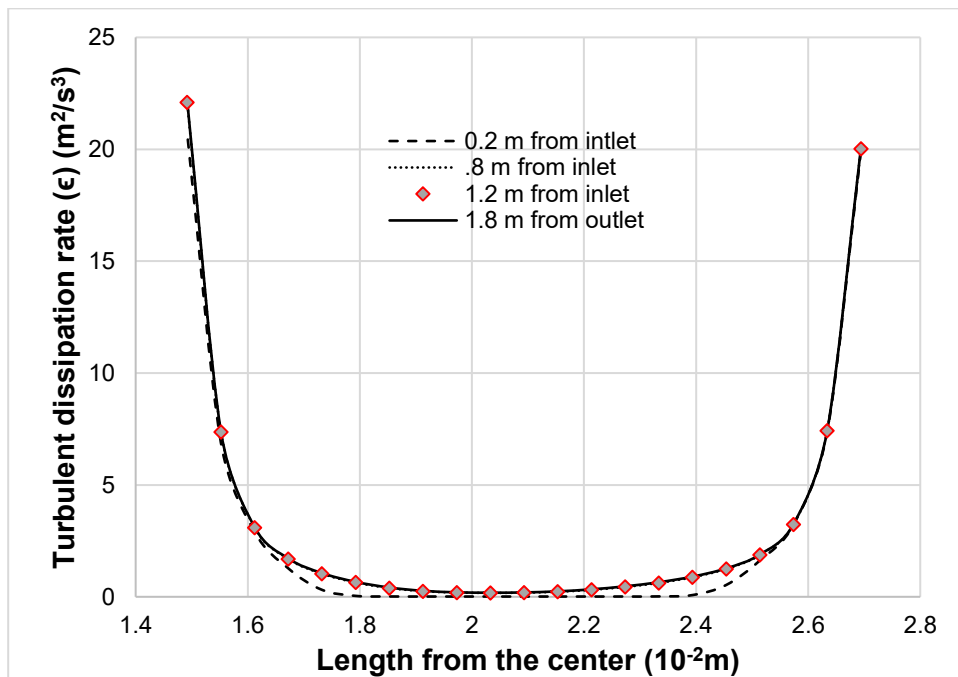he model is higher than that of experimental results. For the bubble and dispersed flow, Caetano's model predicted lower value of pressure gradient than the experimental data and was within the range of 5% error (Caetano et al., 1992). A similar observation is made in current CFD modeling results for bubble and dispersed flow in the annulus. Hence, it can be inferred that the Caetano's model can be used for flow in the annulus for bubble and dispersed flow regime.

Table 4.8 Simulation results for Cateano's experimental data (air-water flow) using VOF approach

Vg (m/s)	V_l (m/s)	Pattern	Simulated Pressure Gradient (Pa/m)	Experimental Pressure Gradient (Pa/m)	Error (%age)	Slip ratio
0.069	1.545	DB	11231	11500	-3%	0.045
0.002	0.0375	BB	7741	7003	10.5%	0.053
0.040	0.090	BB	8340	8859	-5.85%	0.444
0.437	0.101	SL	5056	5086	-0.6%	4.327
1.972	1.959	SL	5783	8459	-32%	1.007
21.893	0.111	AN	1042.5	2254	-48.6%	197.234
16.61	0.523	AN	3574	4671	-23.5%	31.759
21.256	0.111	AN	1008	2125	-52.5%	191.495
16.68	0.548	AN	5115	7685	50.22%	30.438

*DB: Dispersed Bubble, BB: Bubble, SL: Slug, AN: Annular

Next, we used the Eulerian model to simulate the high-velocity flow considering the approach adopted by Parsi et al. (2015) for pipe flow. In order to replicate more realistic conditions, the inlet cross-section is divided into three zones. The gas is introduced from the mid-section while the water is from outer and near the walls as shown in **Figure 4.23**.
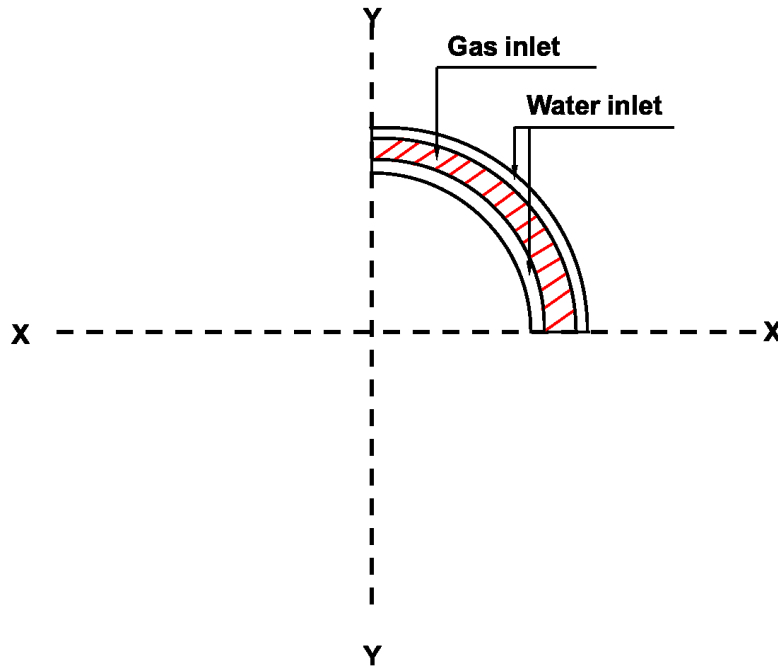

Figure 4.23 Inlet condition for the Eulerian model (Not to scale)

A 2-meter long annular (inner diameter: 0.0422 m and outer diameter: 0.0762 m) flow geometry was constructed using standard mesh module of ANSYS. In the Eulerian model, multi-fluid VOF model with implicit volume fraction parameters was used. In addition, sharp/dispersed type of interface modeling was used. Schiller-Naumann method was chosen to simulate the effect of drag with the drag coefficient of 0.44. Continuum surface force model was selected for surface tension force modeling with 0.072 N/m of surface tension between the phases. k-ε RNG (Re-Normalization Group) model was used as the model for turbulent flow. For this model, default constants of the viscous model were retained, as it has been standard practice in CFD modeling work. Standard wall functions and the turbulent mixing model were also included in the model. The material definition was similar to VOF model as discussed earlier. The three inlets were assigned with velocity-inlet boundary conditions (two for water inlet, and one for gas inlet). The velocity was calculated based on the area of inlet zone. For instance, the velocity in gas inlet zone was calculated using following equation:

$$V_g = V_{g\_given} \frac{A_g}{A_{total}} \tag{4.1}$$

where V_g is the simulation inlet gas velocity for the model, V_{g_given} is the experimental superficial gas velocity, A_g is gas inlet area, A_{total} is total area of the inlet cross-section. It should be noted that the velocity of another phase for the particular inlet is considered to be zero for that particular inlet. For instance, the velocity of water phase is zero in the middle section (gas inlet) and vice-versa. Other boundary conditions were similar to VOF model. Phased Coupled SIMPLE (Semi-Implicit Method for Pressure-Linked Equations) scheme was used for pressure-velocity coupling calculation. For the spatial discretization, different methods were used: (a) Least Square Cell Based for pressure gradient (b) First order upwind for momentum, turbulent kinetic energy, and turbulent dissipation rate, (c) Compressive for volume fraction. In addition, the first order implicit scheme was used for the transient formulation to reduce the computational efforts. It is important to note that the default under-relaxation factors led to a divergence in the model during simulation. Hence, the under-relaxation factors were cut down to different values which are: (a) 0.3 for pressure and momentum; (b) 0.5 for body forces, volume fraction, and turbulent viscosity; (c) 0.6 for turbulent kinetic energy and turbulent dissipation rate; (d) 1 for density. Standard initialization method was used using the inlet conditions. Then, the whole flow domain was patched with the water phase. The time step size was assumed to be 0.001 s with 50 as the maximum allowed iterations for each time step. The volumetric average pressure profile and the void fraction were tracked to monitor the flow development. Finally, the regular convergence criteria were used which 0.001 for all parameters (continuity, k, ε, velocity, and volume fraction). Next, we present the results of the simulations.

In this case, the annular flow pattern for flow in annulus was simulated. The superficial gas velocity and liquid velocity was 13.023 m/s and 0.299 m/s respectively. The experimental results showed that pressure gradient was 3176 Pa/m and the void fraction was 0.81. The volumetric average pressure profile with iterations is shown in **Figure 4.24** and while the void fraction vs.

time-steps is in **Figure 4.25**. The volumetric average of pressure for last 50,000 iterations is 2720 Pa. If we consider this as the average pressure gradient, the error from experimental data is -14.36%. This error is less than the value obtained from the VOF simulation. Similarly, the average void fraction is also within 10 % error range of the experimental data.
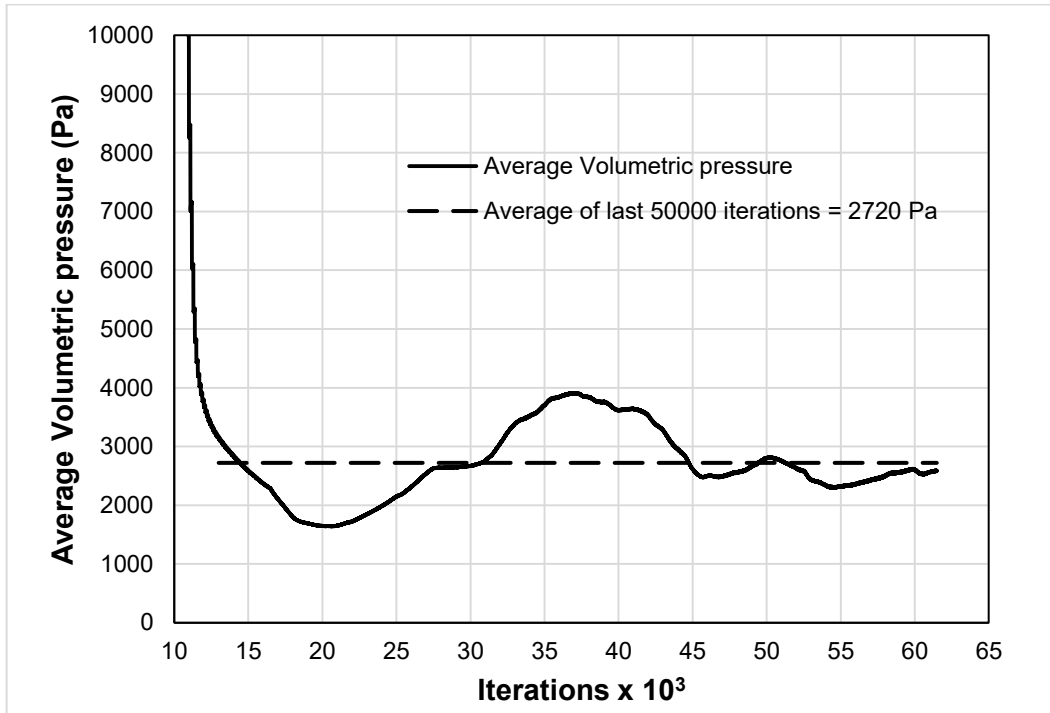

Figure 4.24 Volumetric average pressure with iterations in Eulerian model (The pressure decreases from initial condition and stabilizes with time in the flow domain. The overall average pressure in the test section was 2720 Pa)
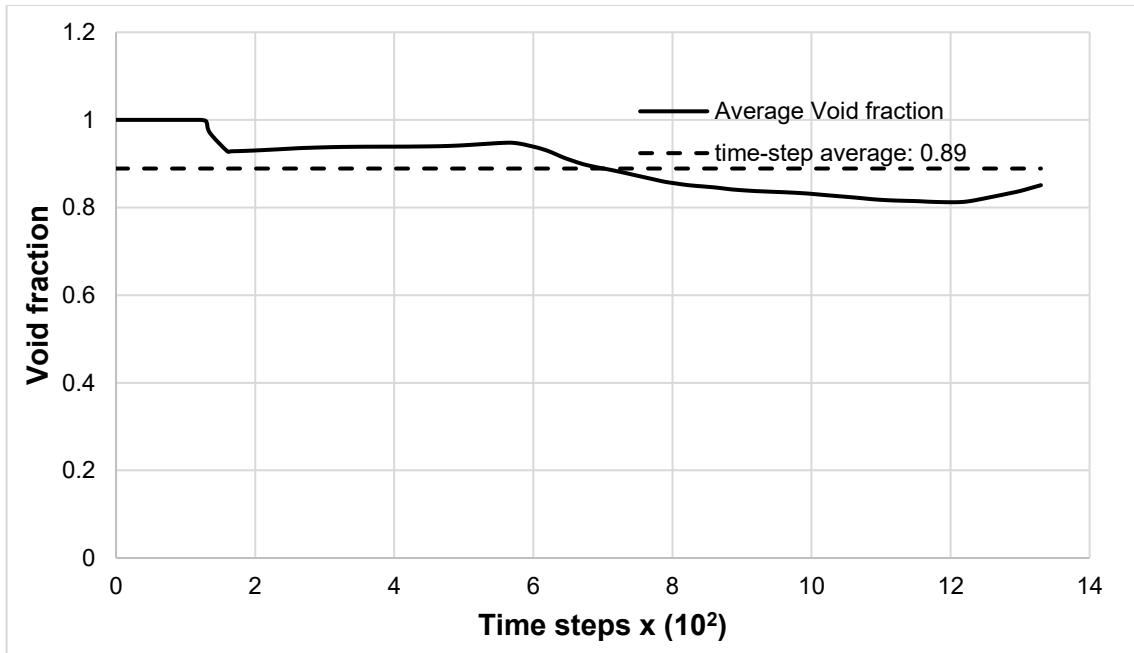
Figure 4.25 Average void fraction variation with time steps (The volumetric average void fraction decreases from the initialized condition and stabilizes with time-steps. The overall average of void fraction in this case is 0.89)

The pressure profile across the length is presented in **Figure 4.26**. The graph suggests that there is an entrance effect in pressure data and which will be more realistic as the mixing of two phases will take place at the inlet. The pressure gradient obtained from simulation was 2486 Pa/m which means that there is deviation of -22% from the experimental data. Error may be introduced in the simulation due to non-inclusion of the factors such as temperature, lift force, and compressibility of air in the system.
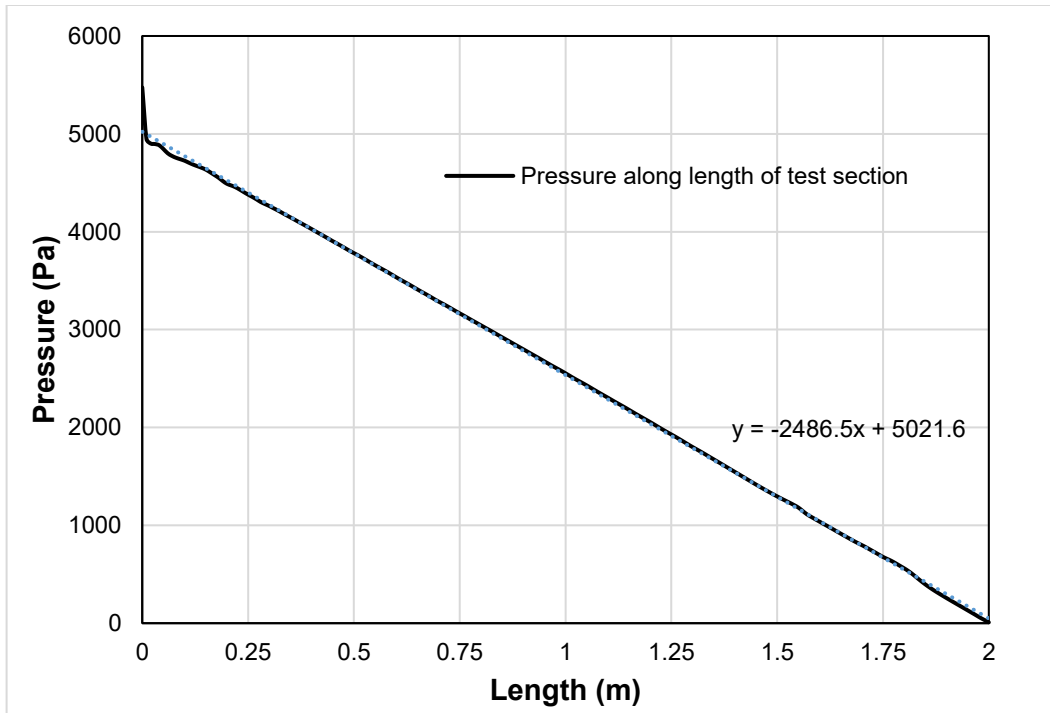
Figure 4.26 Pressure profile in axial direction (The pressure decreases, as we move upward in the annulus)

It is interesting to note the twin peak characteristics of turbulent kinetic energy as shown in **Figure 4.27**. This suggests that when gas is introduced in the mid-section at gas inlet and water along the walls, it creates high turbulent in the system. The presence of water-air mixture exacerbates the turbulent effect. It can be inferred the effect of turbulent is prominent in the high-velocity systems. Also, the contour profile of the void fraction showed a film of water at the wall and the gas in the core of the annulus. Similar observations has been made for the annular flow patterns in past experimental studies.

Figure 4.27 Turbulent kinetic energy variation in radial direction (The turbulent kinetic energy is minimum at the wall and maintains twin peaks across the cross-section. In addition, the energy is lower near the inlet point and becomes constant with height)

Similar observations are made in other cases using Eulerian model. It is important to note that at low velocities and low slip ratios, the results 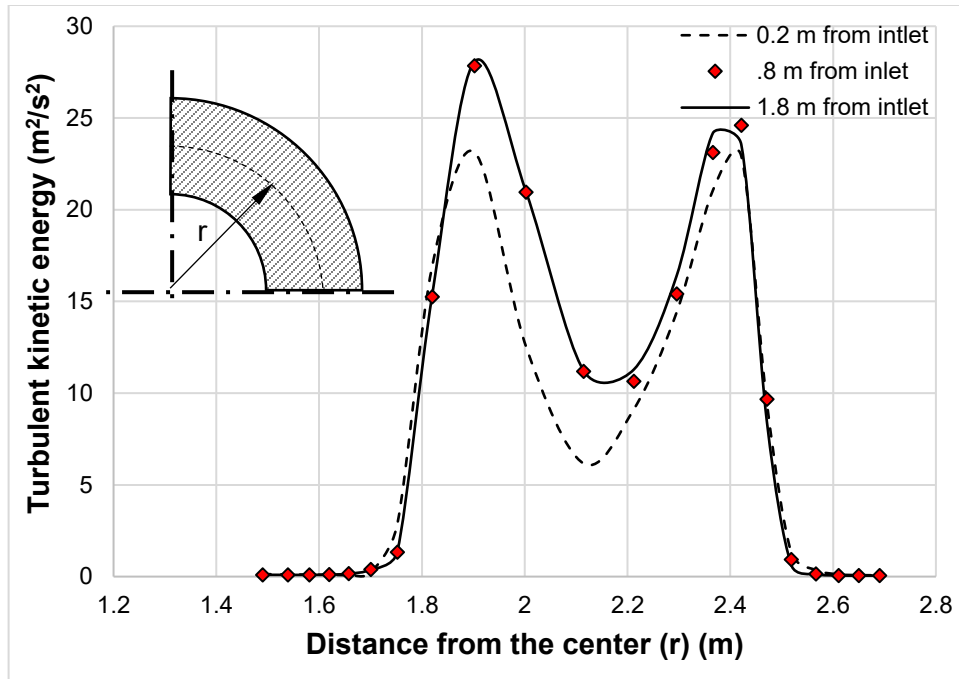were within 1% of the experimental observation. However, similar results are obtained using VOF model at low velocities. Since the VOF model requires a lower computational resource, it is preferred for low-velocity and low-slip-ratio simulation. The pressure gradient and void fraction obtained for other case using Eulerian model are presented in **Table 4.9**.

Table 4.9 Simulation results for Cateano's experimental result (air-water flow) using Eulerian approach

V_g (m/s)	V_l (m/s)	Pattern	Simulated Pressure Gradient (Pa/m)	Experimental Pressure Gradient (Pa/m)	Error (%age)	Slip ratio
0.437	0.101	SL	5056	5086	-0.6%	4.327
13.023	0.299	AN	2486	3176	-22.2%	43

*SL: Slug, AN: annular

4.2.3 Validation of Caetano's Experimental Data for Air/Kerosene

The flow using air and kerosene was simulated with VOF model using the similar approach as the air-water flow was simulated. Only difference in both models were the surface tension values apart from the material properties. The density of kerosene is 780 kg/m³. In case of air-kerosene, the surface tension was assumed to be 0.026 N/m. **Table 4.10** shows the results of different case of air-kerosene flow simulation. It was observed that with increase in slip-ratio, the error in pressure gradient increases. Also, the pressure gradients obtained from the simulation studies is

less than that of the value corresponding to experimental data except the case where gas velocity was lower than the superficial liquid velocity.

Table 4.10 Simulation results for Cateano's experimental result (air-kerosene flow)

V_g (m/s)	V_l (m/s)	Pattern	Simulated Pressure Gradient (Pa/m)	Experimental Pressure Gradient (Pa/m)	Error (%age)	Slip ratio
0.651	2.393	DB	7915	8923	-11.3 %	0.27
0.658	1.197	BB	6424.5	6199	-3.51 %	0.55
4.779	1.994	INT	5563.92	7911.7	-29.7 %	2.4
13.859	0.997	SL/AN	4300.2	6277.8	-31.5 %	13.9
5.571	0.244	CH	1206.05	1816.3	-33.6 %	22.8

*DB: Dispersed bubble, BB: Bubble, INT: Intermittent, SL: Slug, AN: Annular, CH: Churn

4.3 CFD Model for High-Velocity Flow

Apart from the simulation work based on the regular experimental data, few cases were studied where the size of the annulus and pipe were varied. Three cases of different annulus size were considered. The diameter ratio (do/di) was kept constant to compare the flow characteristics. Also, the high-velocity gas case was chosen from Caetano's experimental data. The input velocity parameters in these simulations were: (a) 21.893 m/s as superficial gas velocity (b) 0.111 m/s as superficial liquid velocity. The sizes of four geometries including one from Caetano's experiment is given below.

Table 4.11 Simulation results for high velocity-high diameter flow in the annulus (air-water as two phases)

Casing Inner diameter (in/m)	Tubing outer diameter (in/m)	Simulated pressure gradient (Pa/m)	Experimental pressure gradient (Pa/m)
3 in/ 0.0762m	1.66 in/ 0.0422 m	1042.5	2254
6 in/ 0.1524m	3.34 in/ 0.0844m	463.4	N/A
12 in/ 0.3048m	6.68 in/ 0.1688m	230.13	N/A
22 in/ 0.5588m	12.17 in/ 0.31m	235.34	N/A

*N/A: not available

All the cases were simulated using the VOF model as discussed in Section 4.2.2. The results suggest that for the same superficial gas and liquid velocities, the pressure gradient decreases with the size of the annulus. However, the pressure gradient for 22 in outer diameter was found to be slightly higher than 12 in diameter annulus. This result is preliminary and needs further investigation.

4.4 CFD Model for Current Experimental Setup

4.4.1 Model for Pipe Flow

In this part of the study, the detailed description of the CFD model, which was developed to simulate multiphase flow characteristics (predicting pressure gradient) at high flow velocity,

close to subsonic and sonic velocity will be presented. To carry out the simulation, the fabricated pipe section for University of Oklahoma high velocity flow loop was selected as a modeled flow geometry. The test section consisted of 3.25-in (0.083 m) inner diameter and 17.7 ft (5.41 m) of total length. A schematic of test section which displays the dimensions and locations of pressure sensors and transducer is shown in **Figure 4.28**. Due to the lack of experimental data of pressure loss at high two-phase flow velocity (Ma > 0.3), preliminary CFD model simulations were carried out with anticipated subsonic and supersonic boundary conditions.
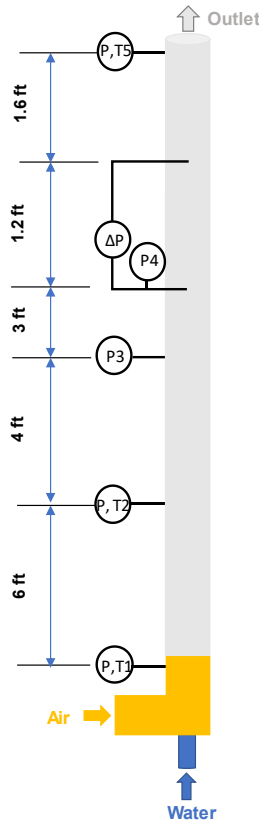

Figure 4.28 Schematic of pipe section for University of Oklahoma high velocity flow loop

A mesh of 116k total number of grids are created over the computational domain using ICEM software and used in ANSYS Fluent. The grid topology of the computational domain is shown in **Figure 4.29**. Unlike the previous simulations, which are presented in Sections in 4.1 and 4.2, these simulations are carried out by accounting for the effect of air compressibility. The primary phase (air) was taken as real gas. In this model, the air properties were modified to account for high Mach number in which air density and viscosity was computed using real gas Peng-Robinson model and Sutherland's law, respectively. In ANSYS package, an explicit form of pressure-based solver was employed to solve 3D transient simulations. A hybrid model (Eulerian-Eulerian model combined with Multi-Fluid VOF model) was selected to model multiphase flow behavior. The Shear Stress Transport (SST) k-ω model was employed to

61

describe the turbulence characteristics of the two-phase flow. In all simulations, the energy equation is activated. Since the pressure-based solver was used to simulate compressible flow, the operational viscous dissipation terms in the energy equation are activated by turning on viscous heating option in the viscous model. For simulation materials, air was specified as primary phase while liquid water was selected as the secondary phase. Water properties were maintained as defined by a default setting in ANSYS. Several phase interaction forces between the two phases (drag, lift, turbulent dispersion, turbulent interaction, and surface tension) were taken into the account. Different models viable in ANSYS package were employed to define these forces. For instance, Schiller-Naumann model is used to define drag force with drag factor of 0.44; Moraga for lift force; Simonin and Troshko-Hassan for turbulent dispersion and turbulent interaction, respectively. In addition, surface tension force was activated and set its coefficient at 72 dyne/cm. Moreover, various options were selected for solving CFD model. Phase coupled SIMPLE method was used for pressure-velocity coupling scheme. Concerning the spatial discretization, the following options were selected: Green-Guess Node Base for gradient; density second order upwind; Momentum third order MUSCL; Volume fraction compressive with bounded second order implicit transient formulation; turbulent kinetic energy and dissipation rate are second-order upwind; and second order upwind for energy. To ensure a converged solution for the simulation, the following under-relaxation factors were selected as: 0.5 for pressure; 0.5 for density; 0.5 for body force; 0.3 for momentum; 0.5 for volume fraction; 0.8 for turbulent kinetic energy and dissipation rate; 0.53 for turbulent viscosity; and 0.6 for energy.
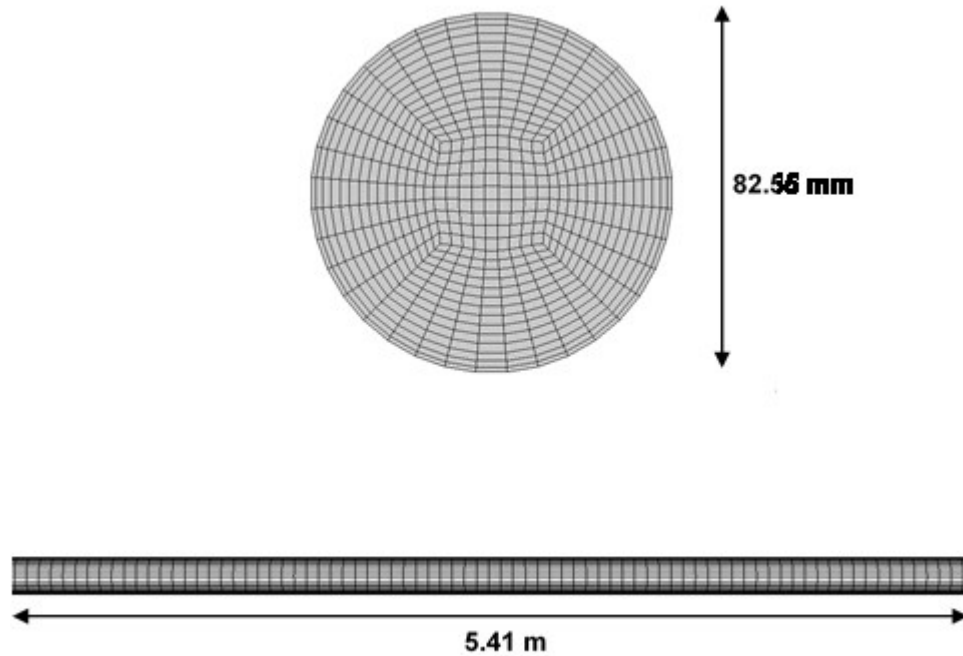
82.55 mm

5.41 m

Figure 4.29 Grid and its topology used to carry out CFD simulations pipe section for University of Oklahoma high velocity flow loop

Boundary conditions of CFD simulation model consisted of three elements. At the inlet pipe boundary condition, a pressure inlet boundary was employed for the mixture. For turbulent parameters, intensity and viscosity ratio specifications were found to be quite useful. On the other hand, a pressure outlet boundary condition was implemented at the outlet of the pipe and set it to zero static pressure. A no-slip boundary condition was specified at the wall with roughness height of 0.0006. An adiabatic condition is also assumed at the wall.

As the initial conditions, the entire domain was assumed to be approximately filled with air phase at zero initial velocity. However, to minimize the computational time, the liquid volume fraction is initiated with 0.1. In all simulations, the time step and a maximum number of iterations per time-step were initially selected to be 0.001 s and 50, respectively. However, the time stepping method was set to variable iteration to ensure the solution convergence. After testing different values of residuals, the maximum residual was set it at 0.001. All the simulations were carried out for at least 1s, which is corresponding to 1000-time steps.

Due to the lack of experimental measurement of multiphase flow at high Mach number, three different arbitrary values of pressure inlet condition 15, 50, and 100 psi were presumed as total gauge pressure to carry out the simulation and determine the possibility of attaining sonic and supersonic conditions. The OU test setup was utilized as flow geometry for all simulations. A 289.24K was nominated as total temperature for both air and liquid water phases. **Figure 4.30** shows the pressure profile along the test section for various inlet pressure values (15, 50, and 100

psi). Simulation predictions evidently reveal the effect of entrance and existence of the test section on the pressure profile, especially at high inlet pressure. As displayed from the figure, the predicted pressure gradually decreases with the length of the test section and rapidly drops to zero at the outlet. The high-pressure drop at the outlet results in sudden expansion, which leads to attaining a high velocity close to sonic (relatively high Mach number). The predicted pressure profile along the test section has been found consistent with previous experimental and theoretical data reported by Henry (1968). However, the pressure profile for the third simulation (100 psi total gauge pressure) doesn't show a smooth trend similar to those at low pressure. Thus, the simulation needs to carry out for a longer time in order to be stabilized. To provide additional validation for CFD predictions, the results of the second simulation case (50 psi) was selected.
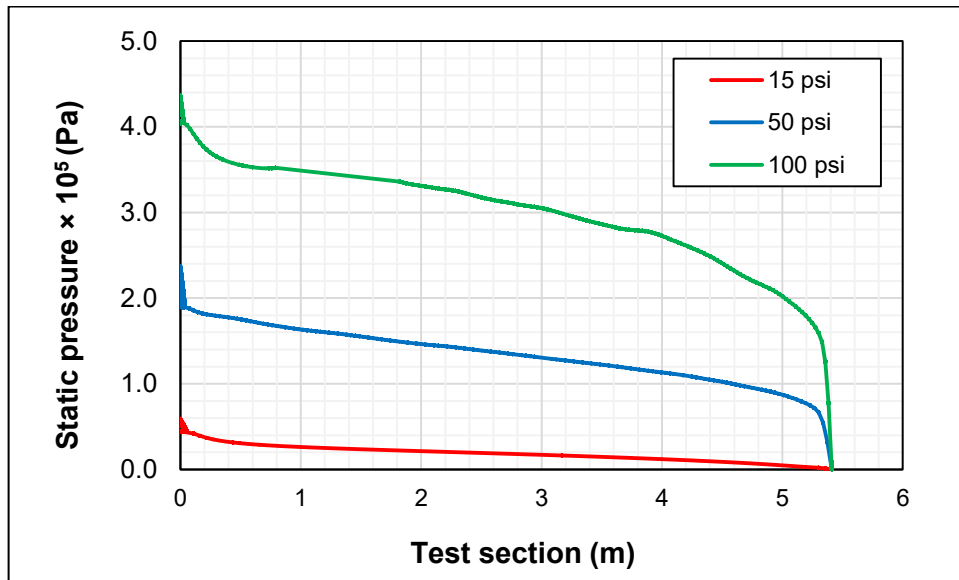

Figure 4.30 Pressure profile along the test section at different inlet pressure values: a) 15 psi; b) 50 psi; and c) 100 psi

Figures 4.31 and **4.32** show the velocity profile, turbulent kinetic energy, and turbulent dissipation rate at different cross-sections (2 and 5.4 m near the inlet). As depicted in Figure 4.31, it shows an anticipated velocity profile for the turbulent flow in the pipe where the flow is not fully developed near the inlet (dot green line). The figure also displays a fully developed velocity profile at 5.4 m near the inlet (solid red line). From this profile, it can be indicated that the maximum velocity is attained at the core of the test section, which is 0.004 m apart from the wall while it reaches to zero at the wall. Additionally, change in the turbulent characteristics (K and ε) through the pipe cross-section and at different heights is presented in Figure 4.32. Apparently, the intensity of kinetic energy and dissipation rate at the mid-section of the test are significantly increased at the outlet due to the high velocity, comparing to their value near to the inlet. At the end of the test section, it is noticed that rate of turbulent dispassion at the core of the pipe is greater than the turbulent kinetic energy.
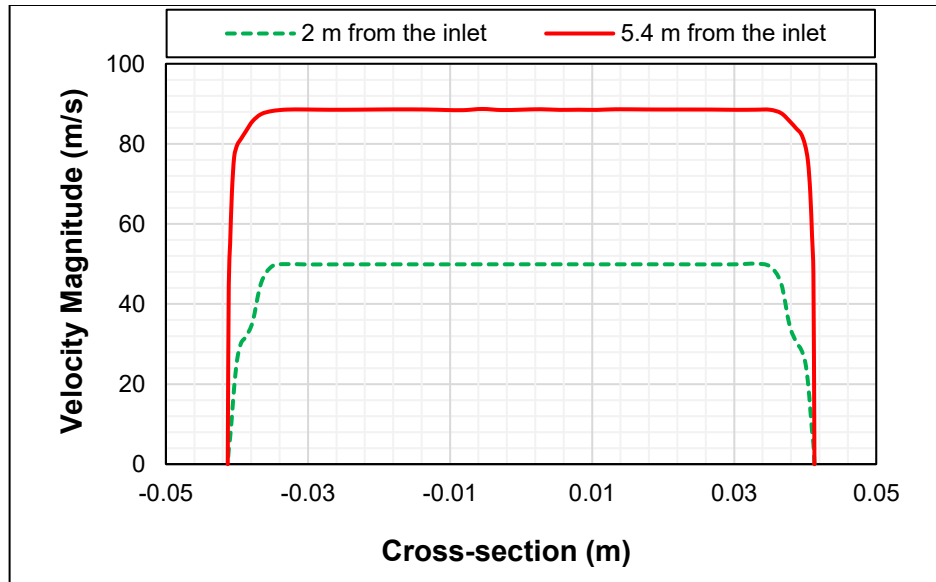
Figure 4.31 Cross-section air velocity profile through 3.25" pipe section
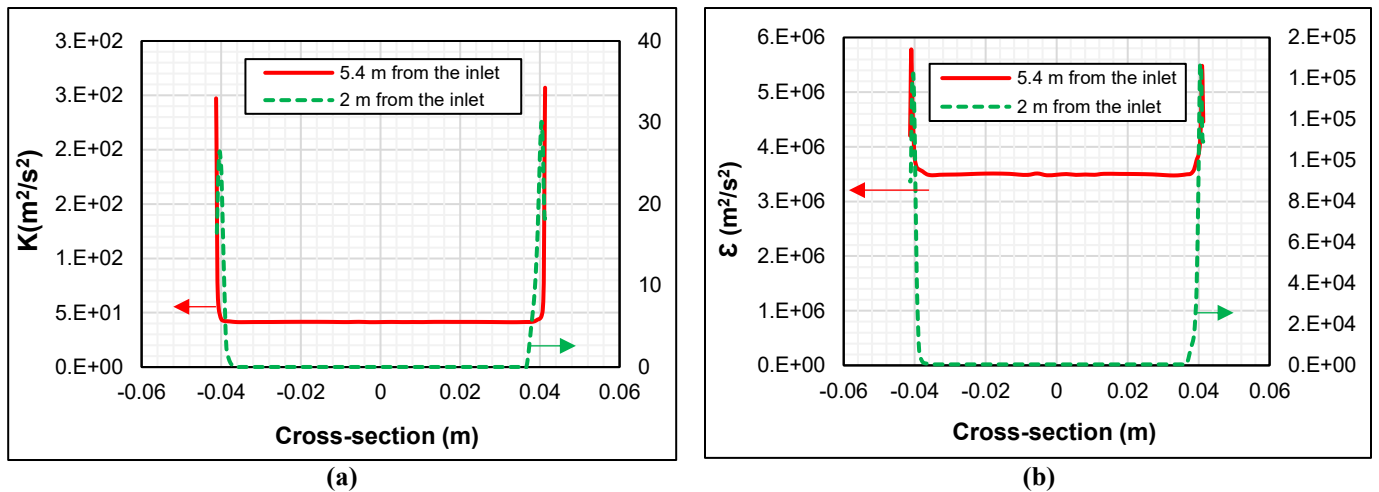

Figure 4.32 Turbulent flow characteristics at two different locations (2 and 5.4 m) from the inlet of 3.25 pipe section: a) Turbulent kinetic energy; b) Turbulent dissipation rate

The variation in the air density and Mach number along the test section is shown in **Figure 4.33**. Typically, density and Mach number trend are relevant to change in the pressure and air velocity trend. Because of the compressibility effect, the air density decreases considerably with a reduction in the static pressure along the test section. The Mach number is basically defined as the ratio of fluid velocity to the speed of sound in the air. Thus, the Mach number is consequently

increasing with the acceleration of the fluid along the test section, attaining its maximum value (approximately 0.27) at the outlet where the peak velocity is observed.
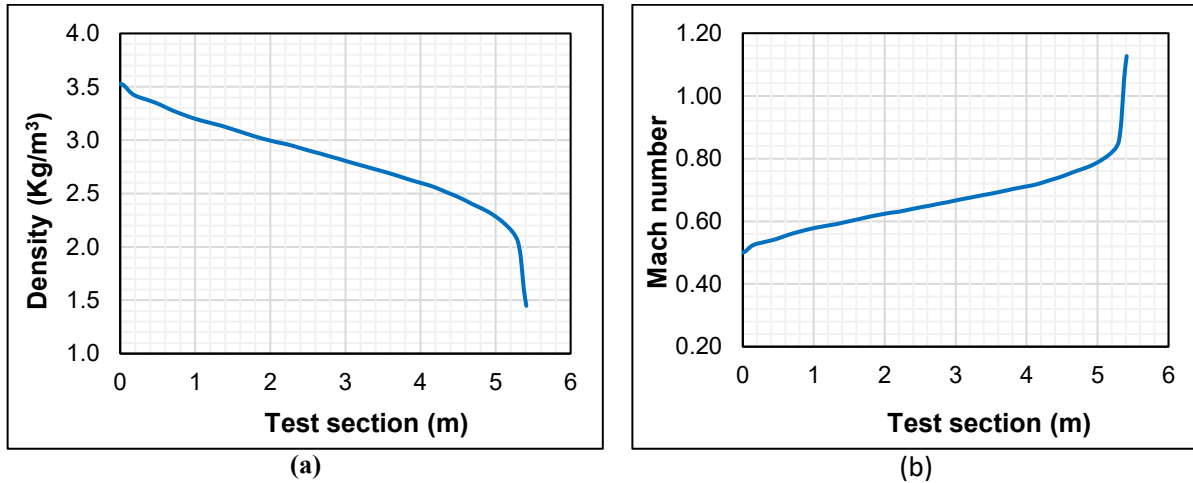

Figure 4.33 Variation of fluid properties and flow characteristics along the test section: a) Density; and b) Mach number

4.4.2 Model for Flow in Annulus

A CFD model was developed for the current laboratory set-up using the Eulerian hybrid model. The geometry was constructed using the quarter cross-section of the annulus as described earlier to minimize the computational cost. The model included the multi-VOF, dispersed phase, and implicit scheme. To characterize the turbulent, k-ω model was used in combination with SST. Also, the dispersed phase was considered for turbulent modeling. The energy equation was invoked to include the compressibility and temperature effect in the system. The fluid considered for two phases were air and water. The real gas Peng-Robinson model with Sutherland model for viscosity was used. Pressure boundary condition was used for inlet and outlet. At the inlet, the range of pressure (14.7-100 psi) was considered, while at the outlet zero total operating pressure was used. The walls (tubing and casing wall) were assigned as stationary with no-slip conditions.

Furthermore, the heat influx from the wall was neglected, since the current lab test section is insulated. The symmetry boundary condition was considered for both XY and YZ planes to reduce the computational time. The inlet condition was used as the reference value for calculation. The pressure-velocity coupling was included by using Coupled scheme in Fluent. For spatial discretization, different schemes were used: (a) Green-Gauss node based method for gradient, (b) third-order MUSCL (Monotone Upstream-Centered Schemes for Conservation Laws) for momentum (c) QUICK (Quadratic Upstream Interpolation for Convective Kinematics) for volume fraction (d) second-order upwind for density, turbulent kinetic energy, specific dissipation rate, and energy. In addition, bounded second order implicit scheme was included for transient formulation. To control the solution convergence, explicit relaxation factors, 0.3 for momentum and 0.5 for pressure was used. In order to avoid convergence in the flow simulation, different under-relaxation factors were used: (a) 0.5 for density, body forces, volume fraction,

turbulent viscosity, and energy (b) 0.6 for turbulent kinetic energy and specific dissipation rate. Several report definitions were specified to monitor the convergence of the simulation. Some of the prominent monitoring parameters were residuals, mass flux, and volumetric average pressure profile with time steps. The calculation was initialized using the inlet conditions. The convergence criteria for residuals were included as 0.001. Variable and fixed stepping was chosen based on convergence pattern of the simulation. The simulation was run till the significant convergence was observed in terms of constant pressure profile, residual and mass flux on the order of 10^{-3}.

The pressure, Mach number, density, turbulent kinetic energy, void fraction, and turbulent dissipation rate along the length is shown in **Figure 4.34-4.39**. As shown in the pressure profile, the pressure reduces sharply at the entrance within 0.5 m from the inlet with a significantly high gradient. The exit pressure is atmospheric. In this case, the Mach number variation ranges from 0.63 - 0.98. Also, a considerable expansion of gas can be seen in the density profile shown in Figure 4.35 (1.2-1.8 kg/m^3). At the inlet condition, the void fraction used as input parameter was 0.9. The void fraction increased from 0.9 to 0.945 with the height of the test section as shown in Figure 4.36. At the entrance, there was a sharp increase in the turbulent kinetic energy and dissipation rate which was reduced to the order of 1 and 1000 respectively within 0.5 m from the inlet. This suggests that when the compressible gas mixes with water it generates high-turbulence in the system, which dissipates over the length.

Note: Figure 4.34 - 4.39 depicts the simulation results from a reference point, which is at distance 19.05 mm in X and Y direction from the origin shown in Figure 4.23.
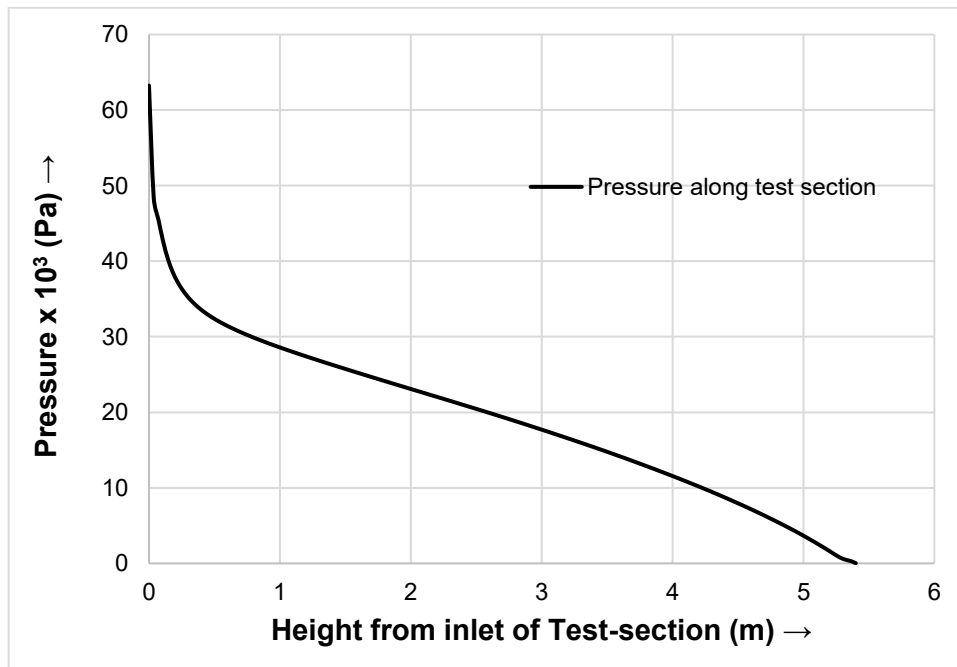

Figure 4.34 Pressure profile along the axial direction of 3.25" × 1.37" annulus at 15 psi as inlet pressure condition (The pressure decreases as we move upward from the inlet point)
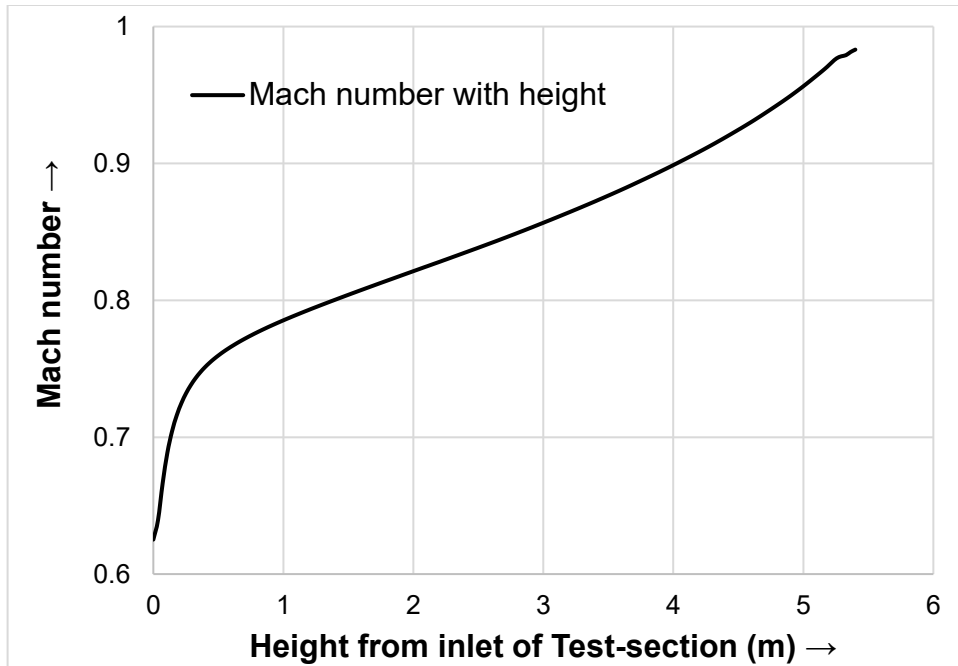
Figure 4.35 Mach number variation in the axial direction for 15 psi inlet pressure condition in 3.25" × 1.37" annulus (Mach number increases with height from the inlet point)
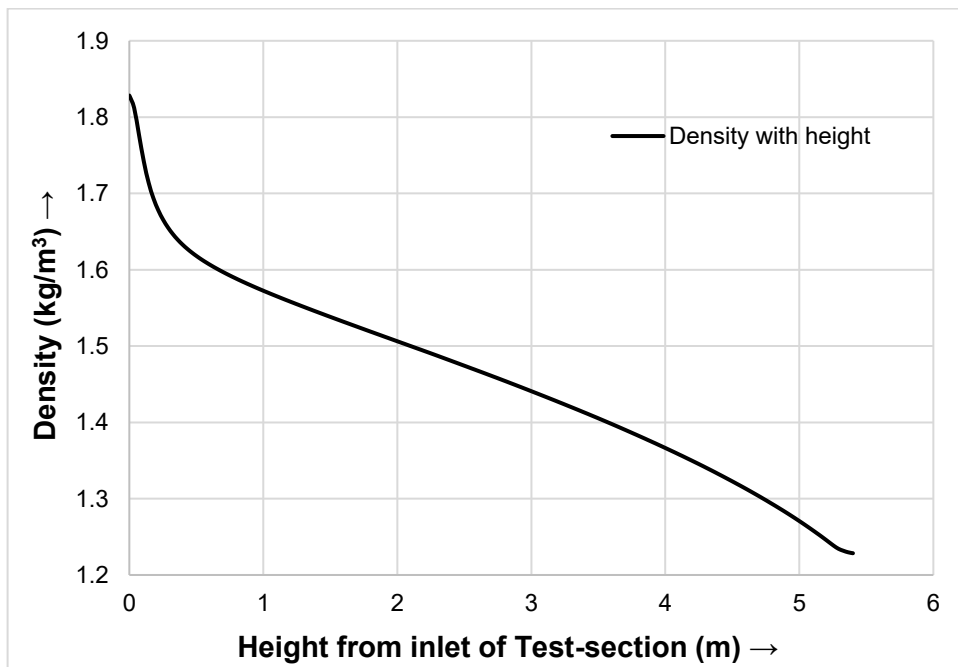

Figure 4.36 Variation of air density in the axial direction of 3.25" × 1.37" annulus for 15 psi inlet condition (The density of air decreases with the height from the inlet of the test section)
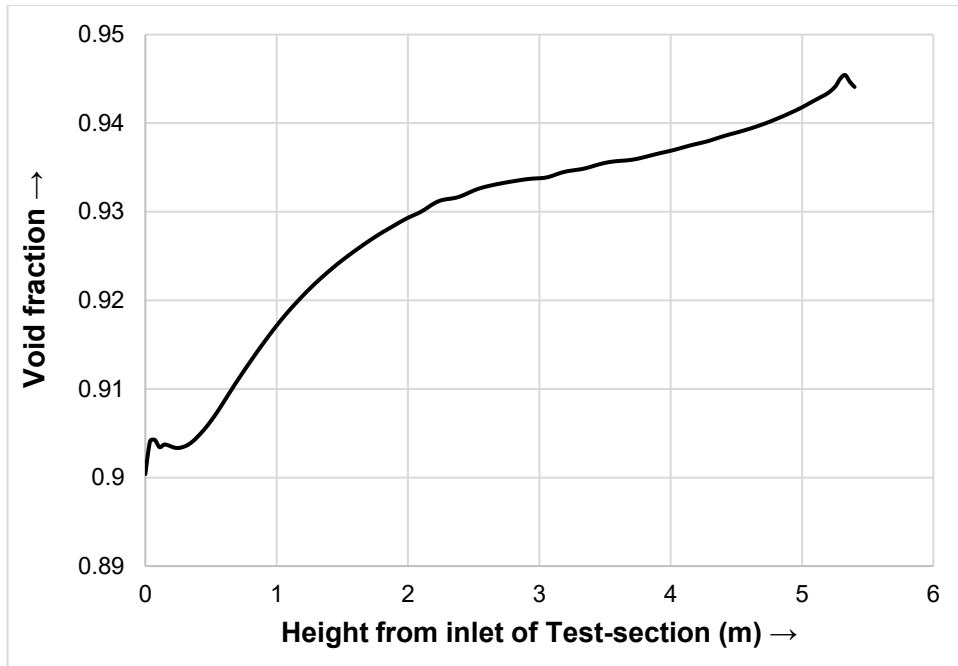
Figure 4.37 Void fraction distribution along the length of 3.25" × 1.37" annulus (The void fraction increases with the height)
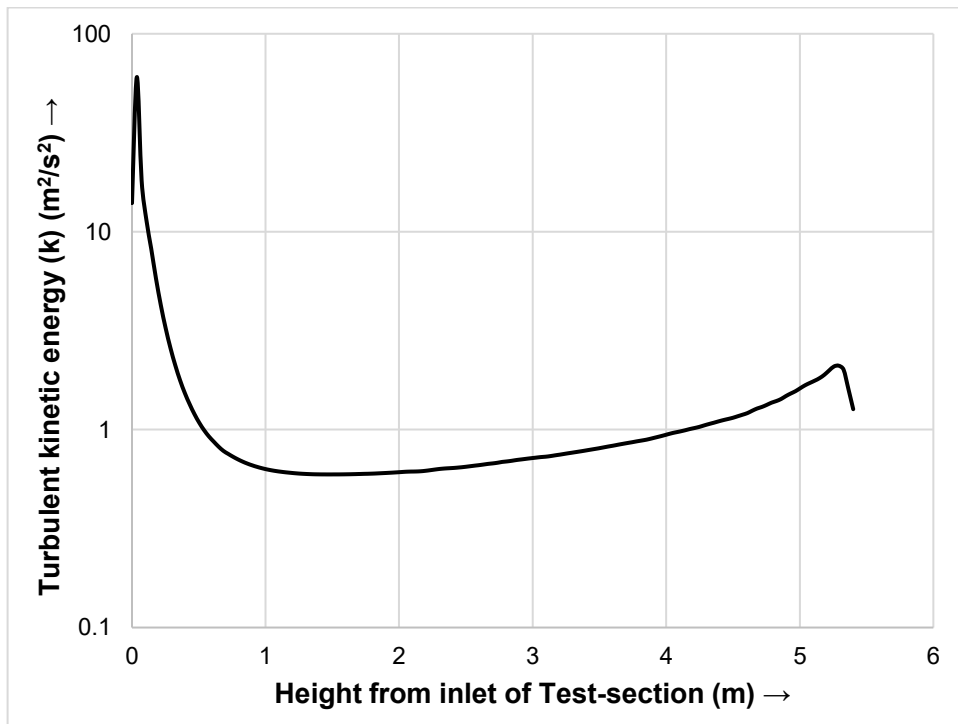

Figure 4.38 Turbulent kinetic energy variation along the axial direction of 3.25" × 1.37" annulus (The turbulent kinetic energy increases sharply at the inlet and reduces significantly with height)
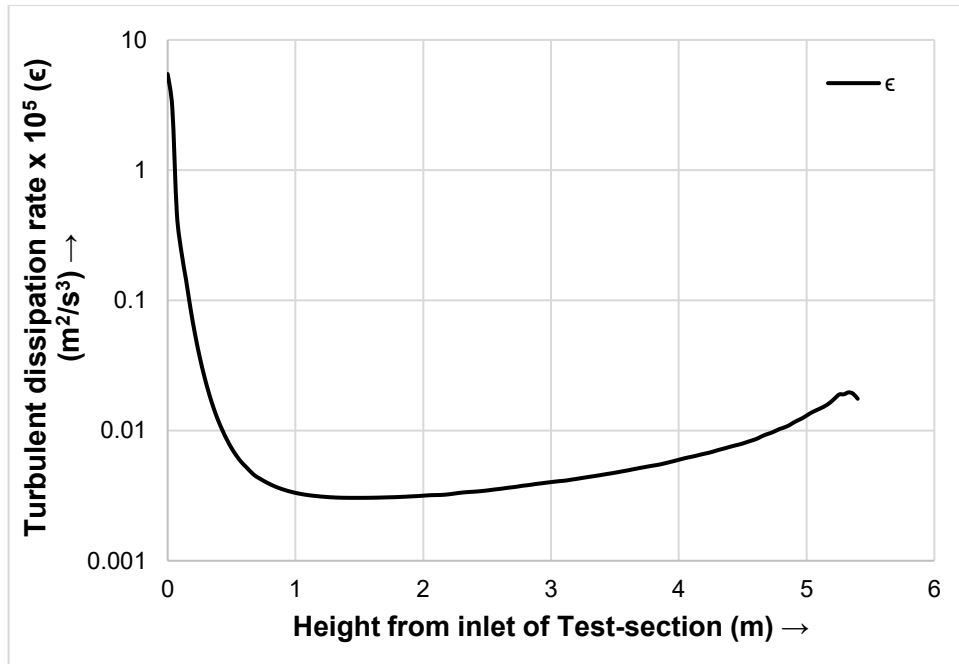
Figure 4.39 Variation of dissipation rate with height in 3.25" × 1.37" annulus (The turbulent dissipation rate is very high at the inlet and reduces significantly with height)

It is worthy to note that the turbulent kinetic energy, and turbulent dissipation rate changes with the radial distance across the horizontal cross sections at a different height. To show this, four cross-sections at different heights from the inlet were chosen: (a) 0.5 m from the inlet, (b) 5 m from the inlet, (c) 5.3 m from inlet (d) 5.35m from inlet. The profiles are shown in **Figures 4.40** and **4.41**. The turbulent kinetic energy is high close to the wall and reduces to zero in the middle part of the annulus section.

Figure 4.40 Variation of turbulent kinetic energy (k) at different cross-sections of 3.25" × 1.37" annulus

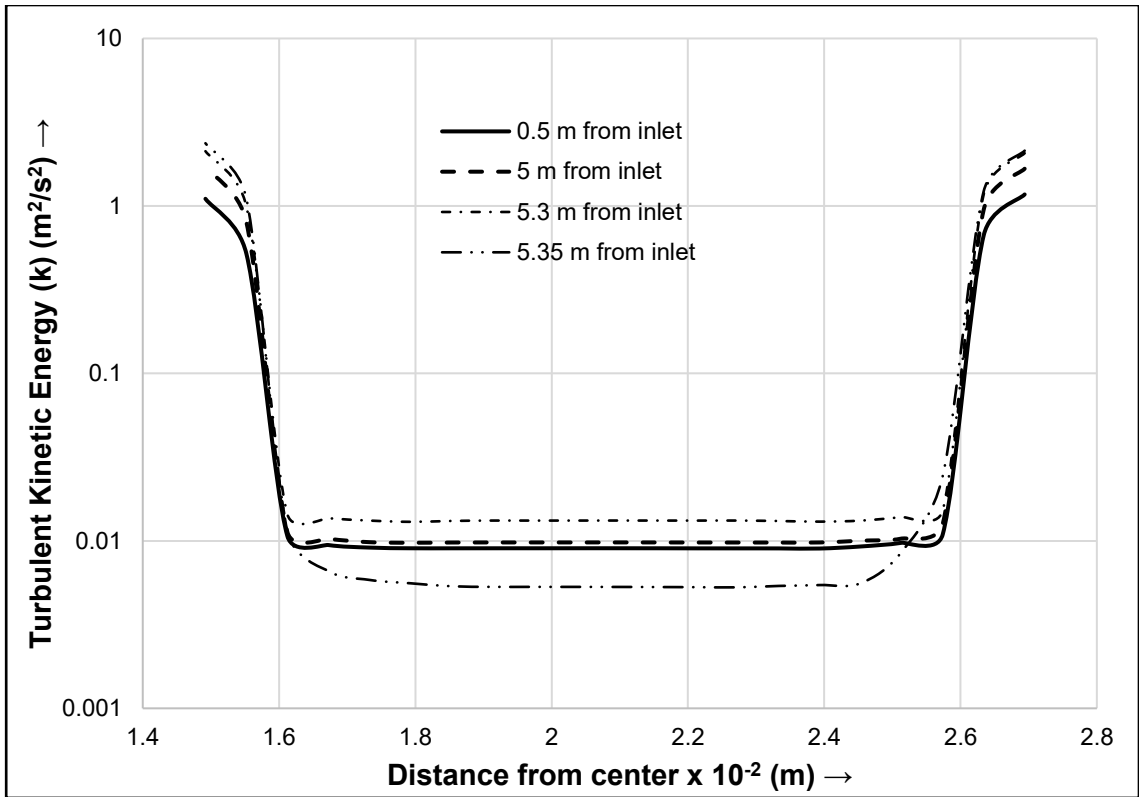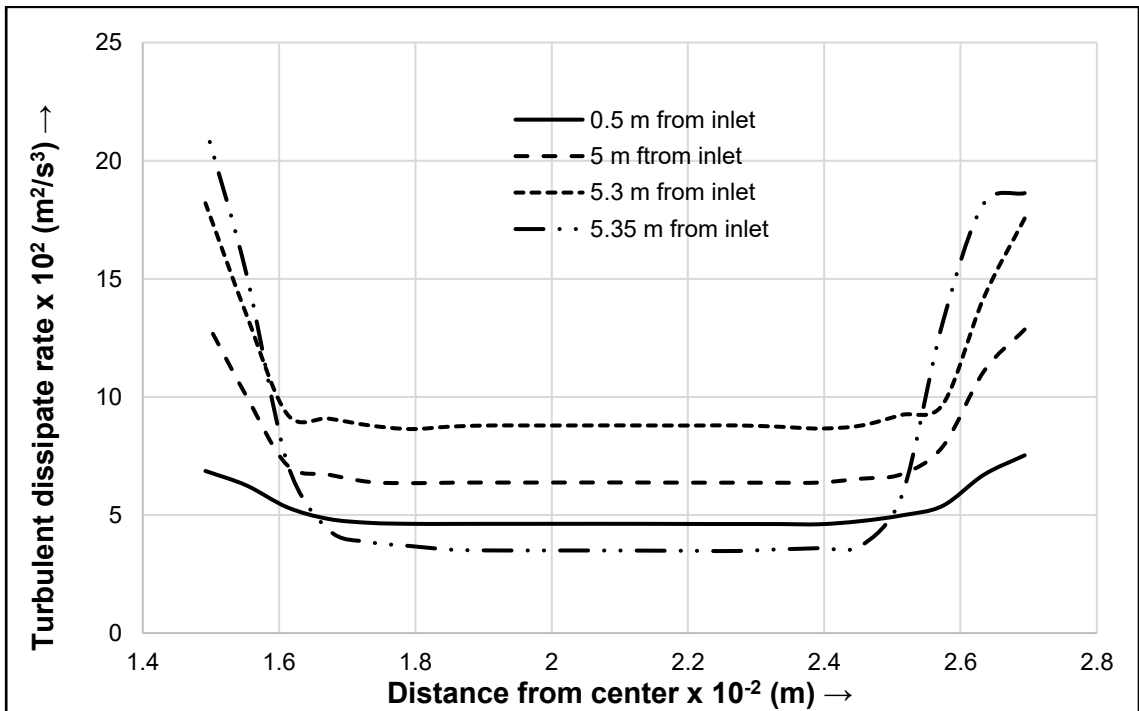**Figure 4.41 Variation of turbulent dissipation rate (ε) at different cross-sectional plane in 3.25" × 1.37" annulus (The turbulent dissipation rate is high along the wall and becomes negligible in the turbulent core. Also, the dissipation rate along the increase with height from the inlet point)**

It can be inferred from Figure 4.40, the velocity of air is zero at the walls of the test section, while in the mid-section it is highest. Opposite trend is observed for the turbulent kinetic energy and dissipation rate which is highest in the vicinity of the wall and the lowest in mid-section. However, the normal pattern for turbulent kinetic energy close to the wall is negligible and in the radial direction, it should have M shaped profile. The inability of capturing the desired profile might be due to unavailability of very thin layered grid structure in the vicinity of the wall. The Mach number profile (Figure 4.35) suggest that the maximum Mach number for 14.7 psi operating pressure is 0.98 is close to the exit. However, it should be kept in mind that ANSYS Fluent calculates the Mach number as ratio of velocity of gas and speed of sound in air. The ANSYS result is adjusted based on the speed of the sound corresponding to air and water volume fraction and the pressure in the flow domain as shown in **Figure 4.42**.
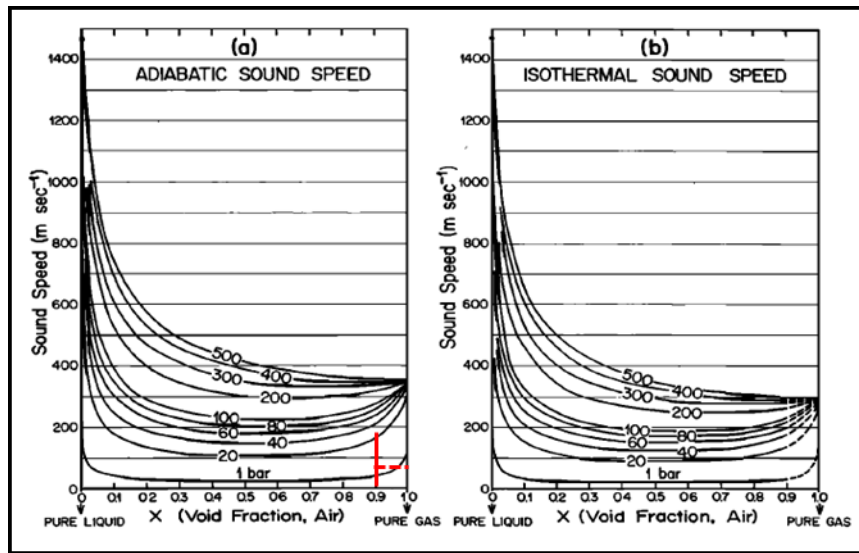
Figure 4.42 Variation of (a) adiabatic and (b) isothermal speed of sound in air-water mixture with gas void fraction and pressure (Kieffer, 1977)

Apart from the 14.7 psi case, two more cases of high velocity are simulated. The cases include the variation of inlet pressure 50 psi and 100 psi with 0.1 as volume fraction of water. The air is introduced at this operating pressure with velocity having 0.7 Mach number. The comparative results of pressure gradient is presented in **Figure 4.43**. The result suggests that there will be two inflection point in the system. One is near the inlet and other is close to outlet. This significant increase in pressure drop also reflects in Mach number and consequently high velocity near the outlet. Similar pressure profile is also reported for the multiphase flow in the nozzle by Henry (1968). The different pressure gradients can provide a useful criterion to develop the WCD tool.
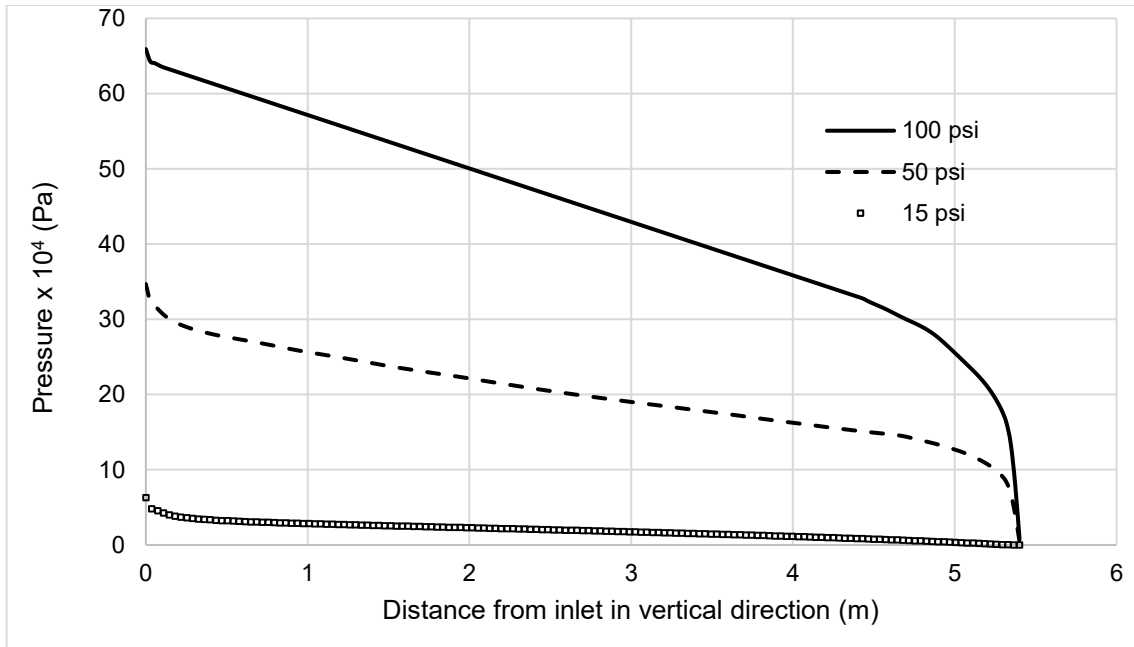
Figure 4.43 Pressure profile for different operating pressure (3.25" × 1.37" annulus)

Figure 4.44 represents the pressure profile for 50 psi pressure gradient and it has three pressure gradient. The pressure gradient at the outlet is highest and approximately twice as that of mid-section. This can also be attributed to high Mach number condition at the exit. The value of pressure gradient at inlet lies in between the values corresponding to the mid-section and top-section.
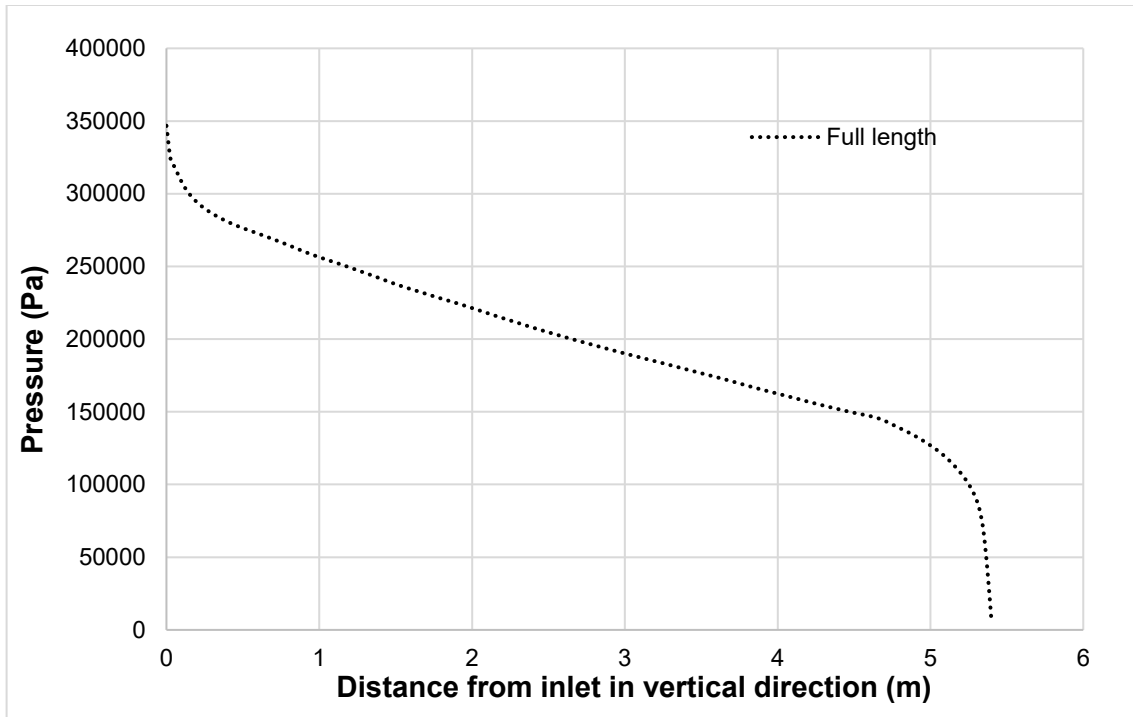
Figure 4.44 Pressure profile for 50 psi operations with different pressure gradients for different parts of test section in 3.25" × 1.37" annulus (highest pressure gradient at the outlet and lowest in the middle part)

The maximum velocity for air corresponding to 50 psi and 100 psi operation pressure was found out to be 120.788 m/s and 170 m/s. As per Kieffer (1977) experimental data (shown in Figure 4.42), the velocity of sound in case of 50 psi (3.44 bar) and 100 psi (6.89 bar) for 0.1 as liquid fraction will be 58 m/s and 154 m/s. This will correspond to the Mach number 2.08 and 1.1 respectively.

4.5 Application of CFD Modeling in WCD Model Development

The whole aim of conducting the CFD simulation to get assistance in WCD tool development. Though CFD modeling has better accuracy than the available empirical, analytical, and mechanistic models, it is computationally intensive. However, it can complement the effort of understanding the flow characteristics, as well as help, identify parameters which will have a noticeable effect on WCD model. CFD modeling results can also assist in gathering more data which can be used to enhance the effectiveness of new WCD models.

The simulation studies suggest that the VOF model can be preferred for low-velocity low-slip ratio conditions in which the error is within 10% limit. The simulation data can be used for testing, validating, and improving predictive tools. It is also observed that CFD results were conservative in nature, and hence it can be the data to be relied upon, unlike the various existing correlations/models. For instance, the Caetano's model for flow in annulus sometime overpredicts the pressure drop which should be taken care of.

In case of high velocity, the error in VOF model increases substantially. The Eulerian model is computationally intensive though simulated void fraction and pressure drop show reasonable accuracy. The Eulerian model is critical to study high velocity multiphase flows, especially annular flow patterns.

In case of high Mach number flows (subsonic and supersonic), the Eulerian model is the most reliable tool. The VOF model was found out to be unable to characterize the compressibility of the gas. The results obtained by Eulerian model needs to be further validated using experimental data. Eulerian model results show three zones in pressure profile. In the vicinity of inlet and outlet, the pressure gradient is significantly higher than that of the mid-section. Highly turbulent mixing was observed near the inlet.

5. Conclusions and Recommendations

Worst-case discharge (WCD) is a complex phenomenon, and it is difficult to address with conventional multiphase flow modeling. An intensive CFD simulation study was performed using ANSYS Fluent to investigate the various characteristics of multiphase flow in vertical pipes and annuli. First, the theoretical background and performance of different multiphase flow models available in ANSYS Fluent were studied to assess their suitability for WCD case. After establishing in-depth theoretical understanding of the models, various cases of multiphase flow that are relevant to WCD were simulated.

It should be noted that the CFD modeling involves significant computational effort. Hence, an attempt has been made to optimize the efforts without compromising the accuracy of results significantly. In pursuit of this, several approaches are outlined and used, such as mesh sensitivity analysis, optimization of simulated pipe/annulus section length, using a quarter sectioned annulus instead of full cross section. Furthermore, different models used during the investigation were validated and verified using published measurements.

Section 4 presents simulation results. Different models (VOF, Eulerian, Eulerian Hybrid and SST k-ω) were used to conduct the simulation work. The models were compared to identify their performance and limitations. The multiphase flow in vertical pipes at subsonic speed was simulated using VOF approach, and flow in annulus was simulated using Eulerian and VOF models. The VOF models showed considerable agreement with the experimental data at low superficial gas and liquid velocities whereas the Eulerian model was found out to be effective at high superficial gas and liquid velocities. In addition, high Mach number (Ma > 0.3) flows were simulated considering the effects of temperature and compressibility on the flow characteristics.

5.1 Conclusions

The main points of this investigation can be summarized as follows:

- The current simulation study suggests that volume of fluid (VOF) and Eulerian model can be used to simulate two-phase flow in pipes and annuli using ANSYS Fluent. VOF model is computationally less expensive as compared to the Eulerian model. However, in high Mach number flows, the effect of compressibility cannot be neglected, and Eulerian Hybrid and SST k-ω models are more effective than the other models.

- The annular pressure drop predictions of VOF model at low-velocities and low-slip ratios show a reasonable agreement with the experimental measurements. The maximum error is within 10% of experimental data. However, at high-velocities and high-slip ratios, the error can be as high as 20%.

- Eulerian model simulation with separate inlets of gas and liquid is capable of characterizing the annular flow pattern in the annulus. It should also be noted that discrepancy between CFD simulation and the experimental measurements could be up to 25%.

- The two-phase air and kerosene flow in the annulus was simulated using VOF model. The difference between the simulated pressure gradient and experimentally measured one is within 35% of the measurement. The discrepancies are on the conservative side of WCD calculation and increase with the slip-ratio.

- For the same diameter ratio and annular superficial gas and liquid velocities, the effect of diameter on annular pressure gradient is minimal when outer diameter is greater than 12 inches.

- Eulerian model in combination with k-ω SST model is capable of simulating high Mach (above 0.3) number of two-phase flows. This model can incorporate the effects of gas expansion and temperature change during the flow in the annulus.

- Simulation results indicated that, in high Mach number two-phase flows (subsonic-supersonic regime), three pressure gradients could be observed along the test section. The highest pressure gradient occurs near the outlet and the lowest in the mid-section.

5.2 Recommendations

- The current simulation work for high-velocity flow needs to be validated with experimental data.

77

References

Abdulkadir, M., Hernandez-Perez, V., Lo, S., Lowndes, I., & Azzopardi, B. J. 2015. Comparison of Experimental and Computational Fluid Dynamics (CFD) Studies of Slug Flow in a Vertical Riser. Experimental Thermal and Fluid Science, 68. pp. 468483. ISSN 0894-1777.

Ali S. F. (2009). Two Phase Flow in Large Diameter Vertical Riser. PhD Dissertation. Cranfield University, School of Engineering Department of Process and Systems Engineering.

Asheim, H. (1986, May 1). MONA, An Accurate Two-Phase Well Flow Model Based on Phase Slippage. Society of Petroleum Engineers. doi:10.2118/12989-PA.

Barati, R. and Liang, J.T., 2014. A review of fracturing fluid systems used for hydraulic fracturing of oil and gas wells. Journal of Applied Polymer Science, 131(16).

Ben Mahmud, H. 2012. Multiphase Transient Flow in Pipes. PhD thesis, Curtin University.

Caetano, E. F. 1985. Upward Vertical Two-phase Flow through an Annulus. Ph.D. dissertation, The University of Tulsa, Tulsa, Oklahoma.

Caetano, E. F., Shoham, O. O., and Brill, J. P. 1992. Upward Vertical Two-Phase Flow through an Annulus—Part II: Modeling Bubble, Slug, and Annular Flow. ASME. J. Energy Resour. Technol. 1992; 114(1):14-30. doi:10.1115/1.2905916.

Chen, P. 2004. Modeling the Fluid Dynamics of Bubble Column Flows. PhD Dissertation, Department of Chemical Engineering, Washington University. http://citeseerx.ist.psu.edu/viewdoc/download?doi=10.1.1.469.8152&rep=rep1&type=pdf

Cook, M. and Behnia, M. 2001. Bubble Motion during Inclined Intermittent Flow, International Journal of Heat and Fluid Flow, Vol. 22, No. 5, pp. 543551.

Da Riva E. and Del Col D. 2009. Numerical Simulation of Churn Flow in a Vertical Pipe. Chem. Eng. Sci., Vol. (64), pp. 3753-3765.

Duns, H., and Ros, N. C. J. (1963, January 1). Vertical Flow of Gas and Liquid Mixtures in Wells. World Petroleum Congress.

Fluent, A.N.S.Y.S., 2016a. Theory Guide 17.2. Ansys Inc. USA.

Fluent User Guide (Version 16.2). 2016b. ANSYS Fluent. Retrieved from http://www.ansys.com/Products/Fluids/ANSYS-Fluent (Accessed on December 22, 2016)

Hasan, A. R., and Kabir, C. S. (1988, May 1). A Study of Multiphase Flow Behavior in Vertical Wells. Society of Petroleum Engineers. doi:10.2118/15138-PA.

Hasan, A.R. and Kabir, CS. 1990. Performance of a Two-Phase Gas/Liquid Flow Model in Vertical Wells, Journal of Petroleum Science and Engineering, 4: 273-289

Henry R.E. 1968. A Study of One- and Two-component, Two-phase Critical Flows at Low Qualities, AEG Research and Development Report (ANL-7430).

Hernandez Perez, V. 2008. Gas-liquid Two-phase Flow in Inclined Pipes. PhD thesis, University of Nottingham.

Hernandez-Perez, V., Abdulkadir, M., and Azzopardi, B.J. 2011. Grid Generation Issues in the CFD Modelling of Two-phase Flow in a Pipe, The Journal of Computational Multiphase Flow, 3, 13 - 26.

Höhne, T. and Lucas, D., 2011. Numerical simulations of counter-current two-phase flow experiments in a PWR hot leg model using an interfacial area density model. International Journal of Heat and Fluid Flow, 32(5), pp.1047-1056.

Hoque, S. Z. and Kalita, P. 2014. Numerical Simulation of Supersonic Viscous Flow over a Flat Plate, International Symposium on Aspect of Mechanical Engineering and Technology for Industry, Nerist, Nirijuli, Volume: 1.

Hossain, M.A., Huque, Z., Kammalapati, R.R. and Khan, S., 2013. Numeric investigation of compressible flow over NREL phase VI airfoil. International Journal of Engineering Research & Technology, 2, pp.1-6.

Hulsurkar, P., Awoleke, O. O., and Ahmadi, M. (2018, March 1). Experimental Study of the Multiphase Flow of Sand, Viscous Oil, and Gas in a Horizontal Pipe. Society of Petroleum Engineers. doi:10.2118/187212-PA

Ibarra, R., Mohan, R. S., & Shoham, O. (2017, August 1). Investigation of Critical Sand-Deposition Velocity in Horizontal Gas/Liquid Stratified Flow. Society of Petroleum Engineers. doi:10.2118/168209-PA

Kieffer, S.W. 1977. Sound Speed in Liquid-gas Mixtures: Water-air and Water-steam. Journal of Geophysical research, 82(20), pp.2895-2904.

Laufer, J., 1954. The structure of turbulence in fully developed pipe flow. NACA Report 1174.

Li, H., Kelecy, F.J., Egelja-Maruszewski, A. and Vasquez, S.A., 2008, January. Advanced computational modeling of steady and unsteady cavitating flows. In ASME 2008

International Mechanical Engineering Congress and Exposition (pp. 413-423). American Society of Mechanical Engineers.

Lien, K., Monty, J.P., Chong, M.S. and Ooi, A., 2004, December. The entrance length for fully developed turbulent channel flow. In 15th Australian fluid mechanics conference (Vol. 15, pp. 356-363)

Lo, S. and Zhang, D. 2009. Modelling of Break-up and Coalescence in Bubbly Two-phase Flows, The Journal of Computational Multiphase Flow, 1, 23 – 38.

Lun, I., Calay, R. K., and Holdo, A. E. 1996. Modelling Two-phase Flows using CFD, Applied Energy, Vol. 53, No. 3, pp. 299-314.

Menter, F.R., 1994. Two-equation eddy-viscosity turbulence models for engineering applications. AIAA journal, 32(8), pp.1598-1605.

Mukherjee, H. and Brill, J. P. (1985). Pressure Drop Correlations for Inclined Two-phase Flow. Journal of energy resources technology, 107(4), pp.549-554. doi:10.1115/1.3231233.

Nikuradse, J., 1933. Gesetzmäßigkeiten der turbulenten Strömung in glatten Rohren (Nachtrag). Forschung im Ingenieurwesen, 4(1), pp.44-44.

Ohnuki, A., and Akimoto, H. 2000. Experimental Study on Transition of Flow Pattern and Phase Distribution in Upward Air-Water Two-Phase Flow along a Large Vertical Pipe. Japan Atomic Energy Research Institute, 319-1195.

Orkiszewski, J. (1967, June 1). Predicting Two-Phase Pressure Drops in Vertical Pipe. Society of Petroleum Engineers. doi:10.2118/1546-PA.

Parsi M., Madhusuden A., Vedanth S., Ronald E. V., Carlos F. T., Brenton S. M., Siamack A. S., Eckhard S., and Uwe H. 2015. Assessment of a Hybrid CFD Model for Simulation of Complex Vertical Upward Gas–liquid Churn flow, Chemical Engineering Research and Design, Volume 105, January 2016, Pages 71-84, ISSN 0263-8762, http://dx.doi.org/10.1016/j.cherd.2015.10.044.

Rui, S.Z. and Xing, Y.M., 2011, March. Numerical Simulation of Two Phase Flow with Evaporation in Supersonic Cross Flow. In Power and Energy Engineering Conference (APPEEC), 2011 Asia-Pacific (pp. 1-4). IEEE.

Sanati, A. 2015. Numerical Simulation of Air–water Two–phase Flow in Vertical Pipe using k-ε Model. International Journal of Engineering & Technology, 4 (1) (2015) 61-70.

Shirdel, M., & Sepehrnoori, K. (2017, February 1). Development of Transient Mechanistic Three-Phase Flow Model for Wellbores. Society of Petroleum Engineers. doi:10.2118/180928-PA

Sorgun, M., Osgouei, R. E., Ozbayoglu, M. E., and Ozbayoglu, A. M. 2011. Gas-Liquid Flow Through Horizontal Eccentric Annuli: CFD and Experiments Compared. In the Proceedings of the ASME-JSME-KSME 2011 Joints Fluids Engineering Conference, Shizuoka, Japan.

Torsvik, A., Skogestad, J. O., & Linga, H. (2017, December 1). An Experimental Study of Gas Influx in Oil-Based Drilling Fluids for Improved Modeling of High-Pressure, High-Temperature Wells. Society of Petroleum Engineers. doi:10.2118/178860-PA

Versteeg, H.K. and Malalasekera, W. 2007. An introduction to computational fluid dynamics: the finite volume method. Pearson Education.

Waltrich, P. J., Hughes R., Tyagi M., Kam S., Williams W., Cavalcanti de Sousa P. Zulqarnain M., Lee W., and Capovilla S. M. 2015. Experimental Investigation of Two-Phase Flows in Large-Diameter Pipes and Evaluation of Flow Models Applied to Worst-CaseDischarge Calculations, BOEM Report M15PC00007, Craft & Hawkins Department of Petroleum Engineering, Louisiana State University, Baton Rouge.

Yancheshme, A., Zarkesh, J., Rashtchian, D., and Anvari, A. 2016. CFD Simulation of Hydrodynamic of a Bubble Column Reactor Operating in Churn-turbulent Regime and Effect of Gas Inlet Distribution on System Characteristics Int. J. Chem. Reactor Eng., 14 (1) (2016), pp. 213-224

Zabaras, G. J, Schoppa, W., Menon, R., and Wicks, M. 2013. Gaps and Advancements for Deepwater Production and Remote Processing: Large Diameter Riser Laboratory Gas-Lift Tests. Offshore Technology Conference. doi:10.4043/23968-MS https://www.onepetro.org/conferencepaper/OTC-23968-MS

Zuber, N. and Findlay, J., 1965. Average volumetric concentration in two-phase flow systems. Journal of heat transfer, 87(4), pp.453-468.